2008

Localized surface plasmon resonance of dielectrically-coated gold nanoparticle arrays

Seyed Mohammad Hashemi Rafsanjani
University of Windsor

Localized Surface Plasmon Resonance of Dielectrically-Coated Gold Nanoparticle Arrays

by

Seyed Mohammad Hashemi Rafsanjani

A Thesis
Submitted to the Faculty of Graduate Studies through
the Department of Physics in Partial Fulfillment of the
Requirements for the Degree of Master of Science at the
University of Windsor

Windsor, Ontario, Canada
2008

Your file Votre référence
ISBN: 978-0-494-47077-0
Our file Notre référence
ISBN: 978-0-494-47077-0

Author's Declaration of Originality

I hereby certify that I am the sole author of this thesis and that no part of this thesis has been published or submitted for publication.

I certify that, to the best of my knowledge, my thesis does not infringe upon anyone's copyright nor violate any proprietary rights and that any ideas, techniques, quotations, or any other material from the work of other people included in my thesis, published or otherwise, are fully acknowledged in accordance with the standard referencing practices. Furthermore, to the extent that I have included copyrighted material that surpasses the bounds of fair dealing within the meaning of the Canada Copyright Act, I certify that I have obtained a written permission from the copyright owner(s) to include such material(s) in my thesis and have included copies of such copyright clearances to my appendix.

I declare that this is a true copy of my thesis, including any final revisions, as approved by my thesis committee and the Graduate Studies office, and that this thesis has not been submitted for a higher degree to any other University of Institution.

Abstract

In this thesis, I study the localized surface plasmon resonance phenomenon in dielectrically coated, closely-spaced gold nanoparticles. I examine the effect of a dielectric coating (that models the sensing of a biomolecular analyte layer) on the optical absorption of these particles. The extinction spectra and the electric field around the particles are calculated. The particles are chosen to be either spheres or hemispheres to be representative of solution phase (3D) or surface (2D) experiments. Calculations are based on the Discrete Dipole Approximation method. In particular, I study the effect of a dielectric coating on the localized surface plasmon spectra around clusters of coated gold nanohemispheres. Based on this study, I propose a new sensing mechanism for detecting biomolecules attached onto a linear array of closely-spaced gold nanohemispheres immobilized on a waveguide surface.

I 'd like take this chance to express my thank for the input I got from various friends and professors. Firstly, I'd like to thank my friend Paul Moffatt for teaching me how to work with LaTeX and how to make many of figures I made in this thesis. I'd like to thank my friends R. Cabrera, A. Senchuk and D. Trojand for their comments and discussions. I am also grateful to Prof. M. Schlesinger for his comments, discussions and points he taught me. I am also very thankful to Prof. Silvia Mittler for her collaboration and points she made about the project. Most importantly I 'd like to express my thanks to my supervisor Dr. Chitra Rangan for giving me the opportunity of working under her supervision, for always being caring, supportive and available for long discussions. It was a great pleasure working under her supervision.

Contents

Author's Declaration of Originality iv

Abstract v

Dedication vi

List of Figures x

List of Appendices xv

1 Introduction 1

1.1 Surface Plasmon Resonance 2

1.2 Localized Surface Plasmon Resonances in Noble-Metal Nanoparticles 5

1.2.1 Effect of Nanoparticle Size 5

1.2.2 The Effect of Ambient Medium 9

1.2.3 Nanoparticles on Surfaces 10

1.2.4 The Effect of Arraying and Aggregation 11

1.2.5 Array Structures that Produce Very Narrow Plasmon Resonances 14

1.3 Electromagnetic Fields around Particles 15

1.3.1 Electric Field around Single Particles 15

1.3.2 Electric Field around Dimers 16

1.3.3 Array Structures that Produce Huge Electric Field Enhancements 17

1.4 Structure of this Thesis 18

2 Methods **19**

2.1 Mie Theory (Exact Solutions) 19

2.2 Approximation Methods 22

2.2.1 Long Wavelength Approximation (LWA) 22

2.2.2 Effective Medium Theories 25

2.2.3 Time-Domain Methods 26

2.2.4 Frequency Domain Methods 27

2.3 Discrete Dipole Approximation (DDA) 28

2.3.1 Mathematical Considerations 29

2.3.2 Dipole Polarizabilities 30

2.3.3 Validity Criteria 31

2.3.4 DDSCAT 32

2.3.5 Computational Complexity and Scaling of DDSCAT 32

2.3.6 Accuracy of DDSCAT 33

3 Results, Discussion and Conclusion **35**

3.1 Effect of a Dielectric Coating on LSPRs in Dimers 36

3.2 Electric Field Calculations around a Dimer 41

3.3 Effect of Aggregation and Arraying 45

3.4 A Novel Biosensing Approach Based on Immobilized Gold Nanoparticles 47

3.4.1 Sensitivity of the Proposed Biosensing Scheme 49

3.4.2 Effect of Nanoparticle's Shape on Biosensing Scheme 49

3.5 Summary of Contributions 56

3.6 Conclusion 56

References **58**

A Copyright Permission **64**

VITA AUCTORIS **66**

List of Figures

1.1 Extinction efficiency vs. wavelength for silver spheres with radii ranging from 20 to 100 nm. Results of Mie theory calculation agrees with calculation in Jensen, et al. J. Cluster Science, 10:295-317, 1999. . . . 7

1.2 Extinction efficiency vs. wavelength for gold spheres with radii ranging from 20 to 100 nm. These are the results of Mie theory calculations. 8

1.3 Extinction efficiency vs. wavelength for a 7 nm gold coated sphere. The coating layer is 1.75 nm thick and n is the refractive index of the coating material. 10

1.4 Extinction efficiency vs. wavelength for a dimer consisting of two silver spheres with radii of 30 *nm*. The separation is center-to-center. The electric field polarization is along the inter-particle axis. Calculations were done using DDA approximation. 13

2.1 The extinction spectra for gold nanospheres with radii ranging from 10 nm to 100 nm. The calculations are done using the MLWA approximation. 24

2.2 Extinction efficiency vs. wavelength for gold spheres with radii ranging from 20 to 100 nm. Comparison of the DDSCAT calculations with Mie theory calculations. 34

3.1 Measured EWA spectra of 40 min-grown nanoparticles of first generation with successively changed polarization in 15 steps: 0 and 180 represent a pure TE (s-polarized) mode whereas 90 represents a pure TM (p-polarized) mode. (top) without coating and (bottom) with a 1,8 octanedithiol SAM. Reprinted figure with permission from Patrick Rooney, Asad Rezaee, Songbu Xu, Touraj Manifar, Abdollah Hassanzadeh, Ganna Podoprygorina, Volker Böhmar, Chitra Rangan and Silvia Mittler, Physical Review B, **77**(23):235446, 2008, Copyright(2008) by American Physical Society. 37

3.2 Calculated extinction spectra for two hemispherical gold nanoparticles with varying interparticle separations. Particles are (top) uncoated in air and (bottom) coated in air. All coatings have a refractive index of 1.45. The particle radius is 7 nm and coating thickness is 1.75 nm. Separation is measured as distance between surfaces, which for coated particles means the coating-to-coating distance. The radiation is in S polarization. Reprinted figure with permission from Patrick Rooney, Asad Rezaee, Songbu Xu, Touraj Manifar, Abdollah Hassanzadeh, Ganna Podoprygorina, Volker Böhmar, Chitra Rangan and Silvia Mittler, Physical Review B, **77**(23):235446, 2008, Copyright(2008) by American Physical Society. 39

3.3 Extinction efficiency vs. wavelength for a dimer consisting of coated and uncoated gold nanohemispheres with radii of 7 nm. The center-to-center separation is fixed at 17.5 nm. The coating layer is 1.75 nm thick. The refractive index of the coating layer is 1.45. The top panel presents S polarization and the bottom panel P polarization. 40

3.4 Schematic diagram of the target and incident field orientation (top). Change in the electric field intensity due to the dielectric coating ($\log[\frac{E_f}{E_i}]$) outside the two nanoparticles and on the plane of support (z=0) of the two nanohemispheres P polarization (bottom) of the incident light. 42

3.5 Change in the electric field intensity due to the dielectric coating ($\log[\frac{E_f}{E_i}]$) outside the two nanoparticles and on the plane of support (z=0) of the two nanohemispheres for S polarization (bottom) of the incident light. 43

3.6 $\frac{|E_f|}{|E_i|}$ at each point on the intersection of the plane of support of two hemispheres and the surface bisecting two hemispheres (at $y = 17.5$). 44

3.7 (top) The geometry of target and radiation's orientation. (bottom) Extinction efficiency vs. wavelength for a cluster of three coated and uncoated gold nanospheres with radii of 7 nm. The coating has a thickness of 1.75 nm and refractive index of n=1.45. The center-to-center separation is 17.5 nm. 46

3.8 (top) The geometry of target and radiation's orientation. (bottom) Extinction efficiency vs. wavelength for a chain of 3 coated and uncoated gold nanospheres with a radius of 7 nm. The coating has a thickness of 1.75 nm and refractive index of n=1.45. The center-to-center separation is 17.5 nm. 48

3.9 A diagram of how particles are placed on the waveguide. 48

3.10 Extinction efficiency vs. wavelength for gold nanoparticle chains with different number of particles, when light polarization is along the inter-particle axis (S polarization) - left two subgraphs, and when light polarization is perpendicular to the waveguide surface (P polarization) - right two subgraphs. The extinction spectra change from the uncoated spectra (a) and (b) to the spectra when coated by a dielectric analyte layer (c) and (d). The radius of all the hemispherical nanoparticles is 7nm and the thickness of coating layer is 1.75 nm. The refractive index of the coating is n = 1.45. The interparticle spacing is 17.5nm center-to-center. 50

3.11 the relative height of the second peak at $\sim 630\ nm$ to the first peak $\sim (530 - 550\ nm)$ vs. the number of particles in the chain. 51

3.12 Extinction efficiency vs. wavelength for a linear chain of four hemispherical gold nanoparticles coated with different coating whose refractive indices ranging between n=1.35 and n=1.55. The particle radius is 7 nm and the thickness of the coating layer is 1.75 nm. The radiation is S polarized. 52

3.13 the relative height of the second peak at $\sim 630\ nm$ to the first peak $\sim (530 - 550\ nm)$ vs. the number of particles in the chain. 53

3.14 Extinction efficiency vs. wavelength for a chain of four gold nanospheres, when light polarization is along the interparticle axis (S polarization) - left two subgraphs, and when light polarization is perpendicular to the waveguide surface (P polarization) - right two subgraphs. The extinction spectra change from the uncoated spectra (a) and (b) to the spectra when coated by a dielectric analyte layer (c) and (d). The radius of all the hemispherical nanoparticles is 7nm and the thickness of coating layer is 1.75 nm. The interparticle spacing is 17.5nm center-to-center. 54

3.15 Extinction efficiency vs. wavelength for a dimer consisting of coated and uncoated gold nanospheres with radii of 7 nm. The coating layer is 1.75 nm thick. The refractive index of the coating layer is 1.45. The center-to-center separation is 17.5 nm. 55

List of Appendices

A Copyright Permission. 64

Chapter 1

Introduction

Gold nanoparticles have been experimentally produced and used for many applications since the time of Michael Faraday [1], who was the first to propose that the color change in auric chloride after adding phosphorus was due to the minute size of the gold particles. Since then, gold nanoparticles have been used in a wide range of applications in medical diagnostics [2], cancer treatment [3], biosensing [4, 5] and biological imaging [6] because of their unique properties that bulk gold does not exhibit. Specifically, there are narrow resonances in the absorption spectrum of gold nanoparticles that are missing from the spectrum of bulk gold. The strong binding affinity of thiol groups [7, 8] to gold allows the functionalization of gold nanoparticles with many organic molecules. This, in addition to the sensitivity of localized surface plasmon resonances to surface modification, makes gold nanoparticles very good candidates for developing biosensors. These sensed molecules can be modelled as a dielectric layer on the gold nanoparticles, and this provides the motivation for this study of the effect of a dielectric coating on gold nanoparticles' plasmonic spectra.

1.1 Surface Plasmon Resonance

When a metal-dielectric interface is irradiated by electromagnetic waves, charge density oscillations are produced on the metal surface. The quanta of these surface-charge oscillations are called surface plasmon polaritons. A "bound" solution at the surface i.e. sustained interfacial waves of plasmons arises when the incident energy is transferred efficiently into the plasmons, and gives rise to the surface plasmon resonance (SPR) phenomenon [9].

In order to qualitatively understand this SPR phenomenon, we must understand the optical (dielectric) properties of a metal. The interaction of a metal with light is dominated by free-electron oscillations. The Drude model of a metal [10] can adequately describe the optical properties of metals in a long range of wavelengths. Briefly, the presence of an electromagnetic field induces an oscillating dipole moment of $\mu = e\mathbf{r}$ in an electron of charge e. Ignoring the effect of the positively charged ions in the lattice, the dielectric constant of the metal is given by Drude expression.

$$\epsilon_{Drude}(\omega) = 1 - \frac{\omega_p^2}{\omega^2 + i\Gamma\omega} \quad , \tag{1.1}$$

where,

$$\omega_p = \sqrt{ne^2/(m_e\epsilon_0)}. \tag{1.2}$$

Here e and m_e are the charge and effective mass of the electrons respectively, ω is the frequency of the driving electromagnetic field. Since photons with appropriate frequencies can drive electrons from inner energy layers into the conduction band, a

better model includes the effect of interband transitions. The contribution of bound electrons to the dielectric function is [10, 11]:

$$\epsilon_{Interband}(\omega) = 1 + \frac{\tilde{\omega}_p^2}{(\omega_0^2 - \omega^2) - i\gamma\omega} \quad , \tag{1.3}$$

where

$$\tilde{\omega}_p = \sqrt{\tilde{n}e^2/m\epsilon_0}. \tag{1.4}$$

Here γ is the damping constant describing radiative damping in the case of bound electrons.

In the surface plasmon resonance phenomenon, the incident electromagnetic wave sets up a charge density oscillation in the metal. These oscillations can be described by the solutions of Maxwell's wave equations at the interface of two different media. For an interface to sustain charge-density oscillations, the following conditions should be satisfied [11]:

$$\epsilon_1(\omega)\ \epsilon_2(\omega) < 0; \tag{1.5}$$

$$\epsilon_1(\omega) + \epsilon_2(\omega) < 0; \tag{1.6}$$

where $\epsilon_1 = \epsilon_1' + i\epsilon_1''$ may be complex. When these conditions are satisfied, the wavelength of the plasmon oscillations on the surface is

$$\lambda_{SPP} \approx \sqrt{\frac{\epsilon_1' + \epsilon_2}{\epsilon_1'\epsilon_2}}\lambda. \tag{1.7}$$

An interface of metal (with complex dielectric function ϵ_1) and vacuum (or dielectric media with real dielectric function ϵ_2) satisfies these conditions at optical frequencies, and therefore charge density oscillations are sustained along a metal-dielectric interface.

When a beam of light with the appropriate frequency is shone on a metal-dielectric interface at an appropriate angle, most of the incident electromagnetic energy is transferred to the surface plasmon modes. At this condition, the reflection from the metal surface is the least [11, 9]. SPR is very sensitive to surface modifications, and presence of biomolecules on the surface can be detected by observing the shift in the peak plasmon resonance angle [12].

In metal nanoparticles, the electron gas is confined to a small ($d \ll \lambda$) three-dimensional volume. The confinement of the plasma to the positively-charged lattice (ions) can be modelled by a restoring force. This results in narrow resonances that are missing from the surface plasmon spectrum of planar gold surfaces [10]. These narrow resonances are called localized surface plasmon resonances (LSPR). LSPR spectra are highly sensitive to the shape and size of the nanoparticle in which the electronic charge density oscillations are excited.

The LSPR is particularly narrow in noble-metal nanoparticles [13] (e.g. silver and gold) and this property has been exploited by using metal nanoparticles for various sensing purposes. Between silver and gold, silver usually has a narrower plasmon resonance but at the same time it is also chemically active which reduces its shelf life. Gold has a slightly wider resonance peak than silver, but has the advantages of being nontoxic and chemically inert. In the following sections, I review the effects of size, shape, separation and dielectric media on the these localized surface plasmons, and on the electric field enhancements around nanoparticles.

1.2 Localized Surface Plasmon Resonances in Noble-Metal Nanoparticles

1.2.1 Effect of Nanoparticle Size

The confinement of plasmon oscillations to a limited space within metal nanoparticles implies the high sensitivity of their surface plasmon resonances to size and geometry. Link and El-Sayed [14] studied effect of nanoparticle's size on the LSPR of gold nanoparticles in water with radii ranging between 9-99 nm. They showed that an increase in nanoparticle's radius leads to a redshift in peak of the plasmon resonance. They also showed that for small particles with ($2r < 45$), increasing the nanoparticle's size leads to a narrowing of the LSPR, while for nanoparticles with $2R > 45$, an increase in the nanoparticle's size broadens the LSPR [14].

Mie [15] was the first to study this size effect quantitatively by solving Maxwell's equations for a sphere irradiated by a plane electromagnetic wave. Figures 1.1, and 1.2 present the extinction efficiency calculations for silver and gold nanospheres with radii ranging between 20-100 nm. As observed in the experiment for gold [14], as the radius of the nanoparticle increases, the peak of plasmon resonance redshifts. Also, the width of the resonance narrows when the nanoparticle size changes from a 40 nm sphere to a 80 nm sphere but for larger particles, the resonance broadens again. These size dependencies can be explained as follows.

To leading order, charge density (or plasmon) oscillations can be described by a dipole, although for oscillations in larger nanaoparticles, higher-order multipolar terms contribute too. Therefore one can classify nanoparticles in two main classes in regard to their size. For small nanoparticles, the scattering cross section is very small and extinction is dominated by absorption. Mie's expression for the extinction cross

section, which is the sum of scattering and absorption cross sections, is given by [13]:

$$\sigma_{ext}(\omega) = \frac{9\omega\epsilon_m^{3/2}V_0}{c}\frac{\epsilon_2(\omega)}{[\epsilon_1(\omega)+2\epsilon_m]^2+\epsilon_2(\omega)^2} \tag{1.8}$$

where ϵ_1 and ϵ_2 denote the real and imaginary parts of the dielectric function of the particle's material, ϵ_m is the dielectric constant of the surrounding medium, V_0 is the particle volume and c is the light's speed. As seen from the above formula, the resonance in the extinction cross section occurs when the denominator is minimum and this condition occurs when $\epsilon_1(\omega) = -2\epsilon_m$. In addition, it is noticeable that within this model there is no size dependence in the extinction cross section except in V_0 which depends on R. It is however, possible to modify the dielectric constant in the previous formula so that $[\epsilon = \epsilon(\omega, R)]$ and import the size dependence into Mie theory [13].

A noticeable size effect emerges as the diameter of the nanoparticles decreases below the mean free path of the conduction electrons which are responsible for plasmon oscillations [16]. Kreibig and et al. [16] used a classical model and argued that when the particle's diameter is smaller than the mean free path (MFP) of the electrons then the dielectric constant of the nanoparticles is no longer the same as the dielectric constant of the bulk material. They showed that the collision frequency ω_0 contains an additional size-dependent term which implies the dependence of optical constants on the size of the particles. Using the size-dependent dielectric constants, they showed that the width of the resonance is proportional to $1/R$ for small particles. The same results was also calculated by Kawabata and Kubo, using a quantum-theoretical model in [17].

For larger nanoparticles ($2R > 45$), scattering becomes increasingly important in the extinction cross section. In addition, as the nanoparticle's radius increases, higher-order multipoles in the charge density distribution contribute to the absorption cross section.

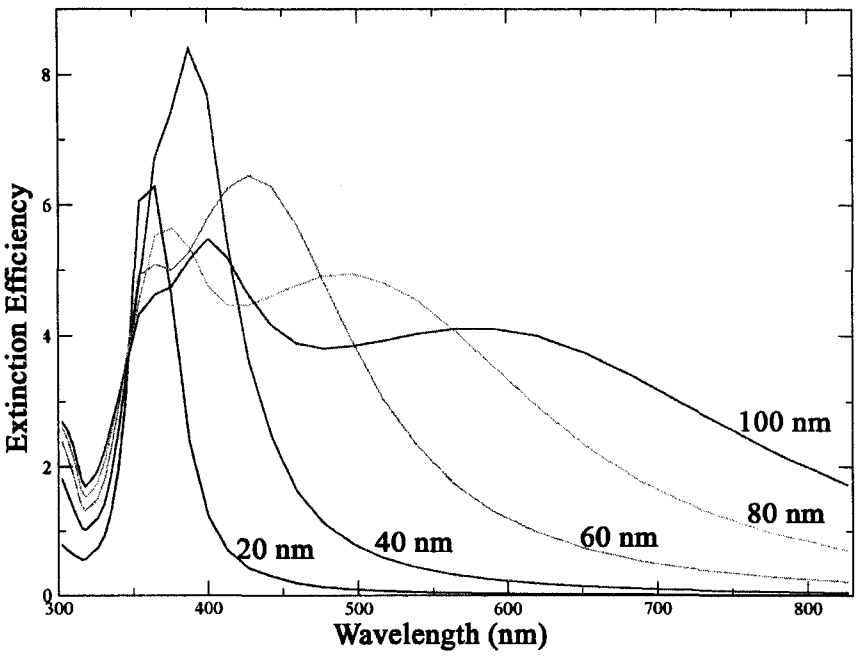

Figure 1.1: Extinction efficiency vs. wavelength for silver spheres with radii ranging from 20 to 100 nm. Results of Mie theory calculation agrees with calculation in Jensen, et al. J. Cluster Science, 10:295-317, 1999.

Ref. [18] calculated the size dependence of the LSPR of silver nanoparticles. Figure 1.1 (that reproduces their results) shows that as a nanoparticle size grows, the resonance band redshifts and broadens. For a 20 nm particle, the peak is at about 370 nm. Fig 1.2 shows my Mie theory calculations for gold. Here also, as particle's radius increases, the resonance band redshifts.

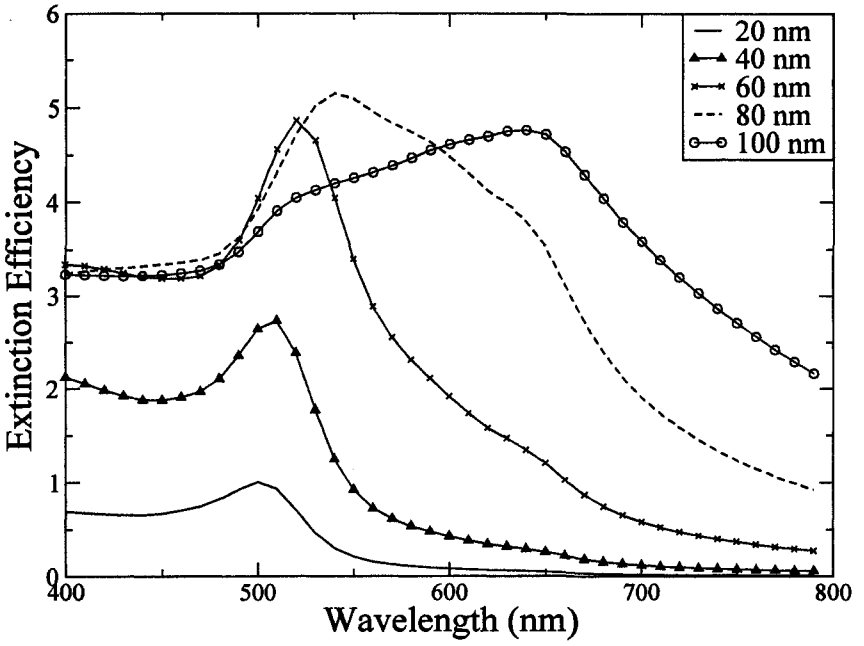

Figure 1.2: Extinction efficiency vs. wavelength for gold spheres with radii ranging from 20 to 100 nm. These are the results of Mie theory calculations.

1.2.2 The Effect of Ambient Medium

Changing the ambient medium (or solvent) around nanoparticles effectively changes the incident radiation's wavelength and the effective dielectric constant of the nanoparticle's materials. Jensen, et al. experimentally [19] studied the effect of an ambient medium on the LSPR of silver nanoparticles. They showed that as the refractive index of the ambient medium increases, the peak of the resonance also redshifts, and there is a linear relation between λ_{max} and the refractive index of the surrounding medium.

One approach to model this effect is using the Maxwell Garnett (M. G.) theory [20] which predicts the optical constants of a medium consisting of metal particles dispersed in a dielectric medium. This theory predicts the relation:

$$\frac{\tilde{n}'^2 - 1}{\tilde{n}'^2 + 2} = q\frac{\tilde{n}''^2 - 1}{\tilde{n}''^2 + 2} \tag{1.9}$$

where $\tilde{n}' = n' - ik'$ is the optical constant of the whole medium and $\tilde{n}'' = n' - ik''$ and q are the optical constant of the metallic particles and the fractional volume occupied by the metal in the composite respectively. Note that if we change the medium, both $\tilde{n}''$ and q change and this leads to a different $\tilde{n}'$.

For spherical nanoparticles, Mie theory [10] predicts the effect of an ambient medium on plasmon resonances as

$$\lambda_{max} = \lambda_p(2\epsilon_{med} + 1)^{(\frac{1}{2})} \cong \sqrt{2}\lambda_p n_{med}. \tag{1.10}$$

Therefore within a window of frequencies where the Drude model is a good approximation, we expect a linear dependency between λ_{max} and the refractive index of medium.

Using Mie theory, makes it possible to study the effect of a coating layer on the LSPRs of single gold particles. Figure 1.3 shows the extinction efficiency calculation

for a 7 nm sphere with a 1.75 nm thick coating on it. The coating material has different refractive indicies ranging from 1 to 1.6. It is seen that placing the additional layer on the sphere leads to a red shift in the resonance which has been previously observed experimentally [21, 22].

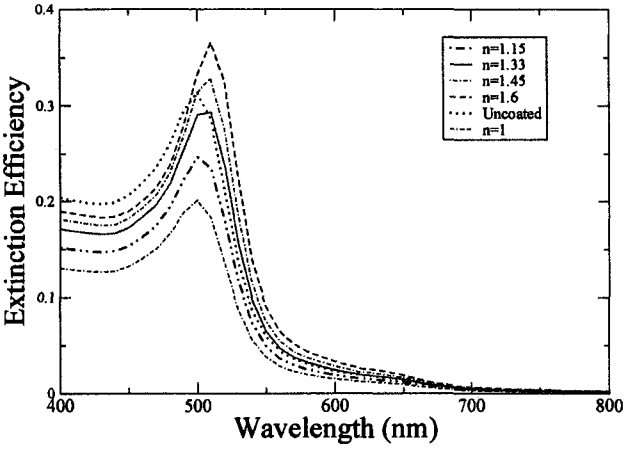

Figure 1.3: Extinction efficiency vs. wavelength for a 7 nm gold coated sphere. The coating layer is 1.75 nm thick and n is the refractive index of the coating material.

1.2.3 Nanoparticles on Surfaces

Nanoparticles can be immobilized on to surfaces by various methods such as self assembly [23, 24], electron beam lithography [25], electroless deposition [26], laser ablation [27], etc. The LSPR of these immobilized nanoparticles are affected by the substrate to various extents depending on the deposition method.

The effect of the substrate has been studied by various researchers. Nillson [28] introduced a method (called R, R', T) to determine the optical constants of metal islands on a substrate by measuring the reflection and transmission of white light from the surface. Marton and Schlesinger [29] introduced and used a modified version of this

method to successfully compute the optical constants of Nickel films. The advantage of their method is the simultaneous determination of an effective thickness with the optical constants. They found that for electrolessly deposited nanoparticles, the substrate plays an important role. Based on Bedeaux and Vlieger's model [30] of granular surfaces, Lazzari and Simonsen developed a software [31] to calculate the linear optical coefficients for nanoparticles on a surface and found that substrates do play a role in LSPR spectra in certain experiments [32].

Malinsky, et al. [33] studied the effect of a substrate on localized surface plasmons in silver nanoparticles both theoretically and experimentally. They predict a linear redshift in λ_{max} with increasing refractive index of substrate. Their calculations overestimate the magnitude of the substrate dependence by almost a factor of two (compared to experiment). In this work, we are modelling nanoparticles that are immobilized on to glass surfaces via silane chemistry [24]. Since the nanoparticles are not directly in contact with the substrate, we can ignore the effect of the substrate in our calculations.

1.2.4 The Effect of Arraying and Aggregation

Spectra of nanoparticle arrays can contain resonance bands that are different from single particle spectra. When two particles are placed close to each other, they make a new target whose optical properties can be different than those of single particles [34, 18]. The reason is simply the interaction between particles.

Simply, the scattered field from one particle changes the incident electric field on the other particle and vice versa. A small enough ($R \ll \lambda$) spherical nanoparticle is, to first approximation, a dipole. Therefore, one of the first problems that should be

addressed is the interaction of two dipoles. A powerful technique to investigate the clustering effect is the generalization of the long-wavelength approximation. That is, we assume that the particles' radii and separation are much smaller than the wavelength of the radiation [13]. For a dimer for example, the resulting dipole moment of each particle is the dipole induced by the electromagnetic field plus a part which is induced by the other dipole.

Realistically, dipoles are not adequate for modelling the charge density oscillations. In order to investigate the interactions in a dimer, Jensen et al. [18] performed accurate calculations of the spectra of two approaching silver spheres. They showed that when the particles are far apart from each other, the spectrum is like that of a single sphere. As the two particles approach each other, the plasmon peak redshifts and a second peak starts growing. Investigating the electric fields around the particles at resonance wavelengths proves that the first peak corresponds to a charge distribution that produces a dipolar field and the second growing peak corresponds to the quadrupolar component. The quadrupolar peak's location is not as sensitive to the particle's separation as it is for the dipolar peak. The most redshifted dipolar peak and highest quadrupolar resonance happens when the spheres are touching.

The inter-particle coupling between two elliptical gold nanoparticles immobilized on a surface has been examined experimentally by Su. et al. [35]. They found a redshift in the peak of the plasmon resonance as nanoparticles approached each other. They also showed that this redshift decays exponentially as the spacing increases. Rooney, et al. [36] studied the effect of nanoparticles separation on much smaller nanoparticles (diameter 14-35 nm). They demonstrated that for particles of this size (14nm diameter), in addition to the red shift of the peak of the resonance, there is an additional peak in the extinction spectrum provided the light polarization is along

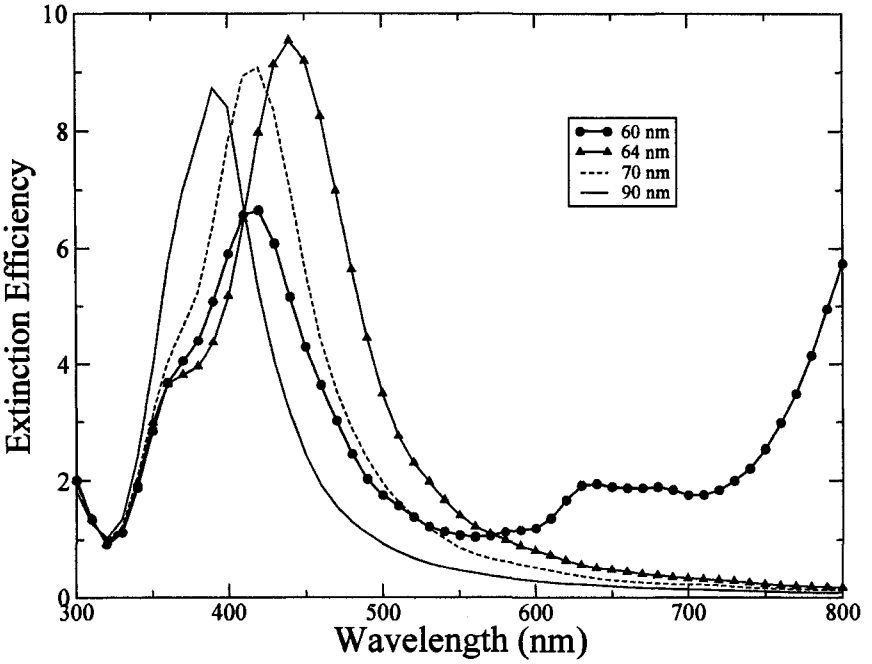

Figure 1.4: Extinction efficiency vs. wavelength for a dimer consisting of two silver spheres with radii of 30 *nm*. The separation is center-to-center. The electric field polarization is along the inter-particle axis. Calculations were done using DDA approximation.

the inter-particle axis. In chapter 3, I show that the presence of the second peak is due an an enhancement of the electric field between the two particles.

Zhao et al. [37] studied the effect of 1D and 2D arraying of nanoparticles on the LSPR spectrum. They showed that for a planar array of silver nanospheres, and radiation polarization parallel to surface, decreasing the spacing can lead to both red shifts and blue shifts depending on the ratio of spacing to particle's diameter. If the ratio of spacing to particle's diameter is bigger than unity then the plasmon resonance peak *blueshifts* as the spacing decreases and if this ratio is smaller than unity then

the resonance *redshifts* as the spacing decreases. In this thesis, I calculate the LSPR of closely-spaced hemispherical gold nanoparticles and the results are presented in chapter 3.

The other important effect is the effect of aggregation (a large number of particles and not in a linear chain). Lazarides and Schatz [38] studied the effect of aggregation for DNA-linked gold nanoparticles in water. They found that for 13nm diameter spheres aggregation of a over a several hundred nanoparticles (particles are 6.5 nm separated) the plasmon peak both redshifts and broadens. Also as opposed to the single particle, aggregates are more efficient light scatterers and scatter most efficiently at a lower frequency band. They showed that to have a large redshift ($\sim 45nm$) aggregates must include over thousand single gold nanoparticles.

1.2.5 Array Structures that Produce Very Narrow Plasmon Resonances

In all the above aggregates and arrays, the interparticle spacing was typically smaller than wavelength. When the interparticle spacing becomes comparable to a single particle's resonant wavelength, there is a dramatic change in the spectrum. Zou, et al.[39] considered the possibility of coherently mixing long-range interactions and the localized surface plasmon phenomenon to produce remarkably narrow plasmon lineshapes. They showed that for a chain of 400×50 nm silver spheres spaced 470 nm apart there is a very narrow resonance at 471.4 nm with a width of only 3.5 nm (20 MeV) provided both the wavevector and light polarization is perpendicular to the chain. It is worth noting that in order to get a considerable long-range interaction, the nanoparticle size should be large enough

Note that the physical reason for this modification of the LSPR is fundamentally different from those of closely-spaced arrays of nanoparticles. While for arrays of spaced on the order of λ, the narrow spectrum is produced via interference, for closely spaced arrays, the spectrum is a signature of the overlap of the induced fields between particles.

1.3 Electromagnetic Fields around Particles

For many spectroscopic applications one needs to study the electric field around particles. At metal surfaces, the electric field is very strong and decays exponentially as one moves away from the metal surface. In Surface Enhanced Raman Scattering (SERS) [40], Raman active molecules attached to the gold surface are excited by the large electric field near the metal surface and the molecule starts radiating. Since the Raman signal is proportional to the fourth power of the exciting electric field, large field enhancements due to a surface or nanoparticles are desirable. Studying the electric field near a nanoparticle's surface can be applied to finding nanostructures that are best suited for SERS applications [41]. This idea has also been used for single molecule detection (SMD) purposes [42].

1.3.1 Electric Field around Single Particles

In the quasi-static regime, when the incident electric field changes much faster than the charge oscillation dynamics, nanoparticles can be modeled as stationary dipoles. Therefore the electric field around a particle can be written as [43]

$$\mathbf{E}_{out} = \mathbf{E}_{inc} - \alpha \left[\frac{\mathbf{E}_{inc}}{r^3} - \frac{3\mathbf{r}(\mathbf{E}_{inc} \cdot \mathbf{r})}{r^5}, \right] \tag{1.11}$$

where α is the polarizability of the particle. The first term is the incident field and the second term is the scattered field outside of the particle to the leading order.

As the particle's radius increases, the dominance of the dipole term is replaced by a combination of dipole + quadrupole. Therefore, the external electric field should also contain quadrupolar corrections. For example, for particles with ($r > 100\ nm$), the electric field also contains radiative corrections. For a dipole (if we ignore other multipolar component of the charge density oscillations) the electric field around particle can be written as [43].

$$\mathbf{E} = k^2 e^{ikr} \frac{\mathbf{r} \times (\mathbf{r} \times \mathbf{P})}{r^3} + e^{ikr}(1 - ikr) \frac{r^2\mathbf{P} - 3\mathbf{r}(\mathbf{r} \cdot \mathbf{P})}{r^5} \tag{1.12}$$

Note that in the limit of $k \rightarrow 0$ this reduces to the static field.

Kelly et al. [43] numerically examined the electric field around Ag spheres. They showed for a 30 nm radius sphere in vacuum, the dipole plasmon resonance and surface averaged electric field enhancement occur at the same wavelength ($\sim$ 369 nm). At this wavelength the surface field intensity enhancement $|E|^2$ is about 30. This so-called "hot-spot", i.e. the point on the surface with the most field intensity enhancement($|E|^2$), is along the polarization direction.

1.3.2 Electric Field around Dimers

One aspect of the electric field around monomers is that the field intensity enhancement is typically less than 10^4. On the other hand, much higher enhancements have already been seen in experiments [44]. Particle aggregation is a necessary condition for such high enhancements, the large enhancement appears to be due to an increase in the local electric field between particles [45].

Hao and Schatz [46] calculated the electric field around dimers of different shapes. They proved that a dimer of 36 nm radius Ag spheres with a 74 nm center-to-center separation provides hot-spots between two particles. The largest enhancements, at

the dipole and quadrupole resonance wavelengths, are 11000 and 3500 times the applied field respectively. These enhancements are much larger that those calculated for single spheres of the same size (by a factor of 10^2). Electric field enhancements of a dimer of Ag nanoprisms (placed tip to tip) were calculated in [46]. It was shown that at the dipolar resonance wavelength ($\lambda = 932\ nm$) the enhancement between two particles is about 53000 times its asymptotic value provided the light polarization is parallel to the surface on which prisms were placed.

1.3.3 Array Structures that Produce Huge Electric Field Enhancements

In Ref.[39], Zou, et al. studied the possibility of mixing localized plasmon resonances and photonic modes of a linear new particle array to produce very narrow plasmon resonances. In such arrays, the resonances appear at wavelengths that are larger than localized plasmon resonances, but the widths and intensities of peaks are correlated to plasmon modes.

It makes sense to expect that by mixing the long range effects and localized enhancements coherently, array structures can support ever higher electric field enhancements. Zou, et al. [47] calculated field enhancements around one dimensional arrays (spacing $\sim \lambda$). Calculations show for a linear array of 400×50 nm (radius) single silver spheres spaced by 470 nm with polarization and wavevector both perpendicular to the array axis the typical enhancements around the central sphere is typically 18 times the enhancements around an isolated single sphere. They also calculated that for an array of spherical Ag dimers a maximum enhancement of $|E|^2 = 3.7 \times 10^4$ can be achieved.

As mentioned earlier, the fact that dimers and nonspherical particles can provide higher enhancements than the single spheres with the same effective radius is a consequence of their low radiative damping. Therefore to produce higher enhancements with long-range effects, spheres are better candidates. At the same time for local plasmons the most enhancements can be achieved with dimers or nonspherical particles (or dimers of nonspherical particles). So the most enhancements can be produced by placing a dimer at the center of a linear array of spheres. Zou, et al. calculated this if the dimer is a dimer of 30 nm (radius) spheres in a chain of 50 nm spheres spaced by 471.4 nm the peak of field enhancement as large as 1.6×10^5 can be produced.

In this thesis, I am interested in field enhancements around an array of closely-spaced nanoparticles coated by a dielectric material. In particular, I am interested in the electric field magnitude between two closely-spaced gold nanoparticles before and after coating with the dielectric layer.

1.4 Structure of this Thesis

In this thesis, I present calculations of extinction spectra of dielectrically-coated closely-spaced gold nanoparticles, and of the electric fields around them. In the second chapter, I discuss various theoretical methods that have been used to investigate the scattering properties of metal nanoparticles, and field enhancements around them.

I specifically discuss in detail the DDA method and its suitability to solve this problem. Chapter 3 contains a study of the effect of a coating on the plasmonic spectrum of a linear array of closely-spaced gold nanoparticles. Based on these calculations, a novel biosensing approach for detecting the presence of biomolecules around a chain of gold nanoparticles is presented.

Chapter 2

Methods

In this chapter, I summarize some of the theoretical methods used to describe the optical properties of noble-metal nanoparticles, i.e. their localized surface plasmon spectra. The mathematical problem is to solve Maxwell's equations for an electromagnetic wave incident on a metal nanoparticle subject to the boundary conditions imposed by the nanoparticle's surface. Specifically, I introduce the Discrete Dipole Approximation (DDA) which is the method used in the calculations presented in the last chapter.

2.1 Mie Theory (Exact Solutions)

An exactly solvable problem in the theory of scattering of light by small particles is that of a sphere of arbitrary radius and refractive index. The Mie solution [15] to this scattering problem is valid for all possible ratios of nanoparticle diameter to wavelength. In its original formulation, Mie assumed a homogeneous, isotropic and

optically linear material irradiated by an infinitely extending plane wave. However, solutions for layered spheres, spheroids and infinite cylinders were also developed [10]. Although Mie's solution only works for certain geometries it can also be used as the first approximation of optical effects in nonspherical particles, particularly in size effect studies.

The main features of Mie theory are explained below and a complete treatment can be found in [10]. The main goal is to solve Maxwell's electromagnetic field equations written in the following form:

$$\nabla^2\mathbf{E} + k^2\mathbf{E} = 0, \quad \nabla^2\mathbf{H} + k^2\mathbf{H} = 0.$$

Here E is the electric field component of the electromagnetic wave and H is the magnetic field component of the electromagnetic wave. The wave vector of the light, k, is related to the frequency ω through the dispersion relation $k^2 = \omega^2\varepsilon\mu$; where ϵ, μ are the dielectric constant and permeability of the sphere's material. Equivalently, one can prove that if ψ is a scalar function that satisfies the equation $\nabla^2\psi + k^2\psi = 0$, then the vector functions $\mathbf{M}, \mathbf{N}$ where

$$\begin{aligned} \mathbf{M} &= \nabla \times (\mathbf{r}\psi), \\ \mathbf{N} &= \frac{\nabla \times \mathbf{M}}{k}, \end{aligned} \tag{2.1}$$

are the solutions of Maxwell's equations as well [10]. The function ψ is called a generating function for the vector harmonics $\mathbf{M}$ and $\mathbf{N}$. The scalar wave equation is separable in spherical coordinates:

$$\psi(r,\theta,\phi) = R(r)\Theta(\theta)\Phi(\phi), \tag{2.2}$$

$$\frac{d^2\Phi}{d\phi^2} + m^2\Phi = 0, \tag{2.3}$$

$$\frac{1}{\sin\theta}\frac{d}{d\theta}\left(sin\theta\frac{d\Theta}{d\theta}\right) + \left[n(n+1) - \frac{m^2}{\sin^2\theta}\right]\Theta = 0, \tag{2.4}$$

$$\frac{d}{dr}\left(r^2\frac{dR}{dr}\right) + [k^2r^2 - n(n+1)]R = 0. \tag{2.5}$$

Here, m, n are determined by angular conditions that ψ must satisfy. For example, ψ must be a single-valued function of the azimuthal angle ϕ. The solution of the radial equation is a linear combination of Bessel functions $j_n(kr)$ or $y_n(kr)$. For the Θ, component the solutions are Legendre polynomials. The generating functions that satisfy the scalar wave equation in spherical polar coordinates are:

$$\psi_{emn} = \cos(m\phi)P_n^m(\cos\theta)z_n(kr) \quad , \quad \psi_{omn} = \sin(m\phi)P_n^m(\cos\theta)z_n(kr), \qquad (2.6)$$

where $z_n(kr)$ is any of the four spherical Bessel functions $j_n, y_n, h_n^{(1)}, h_n^{(2)}$ and the subscripts o and e represent odd and even solutions respectively. From these, and by using equations 2.1, the vector functions **M** & **N** can be obtained. If we expand the incident electromagnetic field in terms of **M** & **N**, and impose the boundary conditions on the surface of the sphere and at infinity, we obtain expressions for the internal and scattered fields. Having the electromagnetic fields in hand, we can find the scattering and extinction cross sections:

$$C_{sca} = \frac{2\pi}{k^2}\sum_{n=1}^{\infty}(2n+1)(|a_n|^2 + |b_n|^2),$$
$$C_{ext} = \frac{2\pi}{k^2}\sum_{n=1}^{\infty}(2n+1)Re\{a_n + b_n\},$$

where

$$a_n = \frac{\mu m^2 j_n(mx)[xj_n(x)]' - \mu_1 j_n(x)[mxj_n(mx)]'}{\mu m^2 j_n(mx)[xh_n^{(1)}(x)]' - \mu_1 h_n^{(1)}[mxj_n(mx)]'},$$
$$b_n = \frac{\mu_1 j_n(mx)[xj_n(x)]' - \mu_1 j_n(x)[mxj_n(mx)]'}{\mu_1 j_n(mx)[xh_n^{(1)}(x)]' - \mu_1 h_n^{(1)}[mxj_n(mx)]'}.$$

Here $x = \frac{2\pi Na}{\lambda}$, $m = N_1/N$, a is the radius of sphere, N is the refractive index of medium, and λ is the wavelength. In the above formula, the prime indicates a differentiation with respect to the argument in parentheses. Absorption cross section C_{abs} can be found by using the relation $C_{abs} = C_{ext} - C_{sca}$.

The treatment of this problem can be modified to solve the problem of a sphere with a coating on it [15]. I used a FORTRAN implementation [10] of Mie solution to study the effect of a coating and ambient medium on the localized surface plasmon spectrum of a spherical gold nanoparticle, and to verify the numerical accuracy of my other calculations done using DDA.

2.2 Approximation Methods

As soon as we consider non-spheroidal particles or a cluster of particles, an analytical solution is not available and numerical approximations have to be made. These approximations allow for elegant solutions that provide physically intuitive explanations and/or for numerical implementations that can be compared with experimental data.

2.2.1 Long Wavelength Approximation (LWA)

Provided particles are much smaller than the light's wavelength one can use an electrostatic treatment (solve Laplace's equations) as a highly accurate approximation. The main advantage of this approach is the fact that Laplace's equation is an analytically solvable equation for a wide range of geometries. A detailed description of the LWA can be found in [48, 34]. For the simplest case, assuming the particles are spherical, by solving Laplace equation we can find the induced polarization,

$$\mathbf{P} = \alpha \mathbf{E}, \tag{2.7}$$

where r is the sphere's radius and the polarizaility α is given by

$$\alpha = r^3 \frac{\epsilon - 1}{\epsilon + 2}. \tag{2.8}$$

This implies that the single-particle resonance occurs when $Re\ (\epsilon + 2) = 0$. However, we know that plasmon resonance and its bandwidth are both size dependent. This

theory can be extended to contain size dependence by adding an additional incident electric field to contain radiative correction terms. Therefore equations 2.7 have to be changed to

$$\mathbf{P} = \alpha[\mathbf{E} + \mathbf{E}_{rad}], \qquad \mathbf{E}_{rad} = \frac{2ik^3}{3}\mathbf{P} + \frac{k^2}{r}\mathbf{P}. \tag{2.9}$$

The first term in $\mathbf{E}_{rad}$ describes *radiative corrections* [49] and is chosen to describe the power that the induced dipole loses due to radiation [50]. This radiative damping term is proportional to $k^3 \times$ (the volume of the particle) and is of the order of unity when the particle's radius becomes comparable to the light's wavelength. This term grows rapidly as the particle's radius increases. For optical frequencies and gold particles with a radius smaller than 100 *nm*, the dominating corrective term is the second term. This second term, describes *dynamic depolarization* [18] that comes from depolarization of the radiation across the particle's surface due to the finite ratio of particle size to the wavelength of the radiation. This depolarization term is the dominating corrective term in smaller particles and causes the red shift and broadening of the plasmon as nanoparticle's size increases. For larger particles, radiative damping starts playing as considerable of a role as the *depolarization* term. This rectified version of LWA is called [34] the modified long wavelength approximation (MLWA).

Fig. 2.1 shows the extinction spectra for gold nanospheres with radii ranging between 10 to 100 nm. Comparing with Fig. 2.2, we see that MLWA works well for smaller particles whose spectra is governed by dipolar component. However this method does not work as well for larger particles. It misses the higher multipolar contributions because we simply assumed our target is a dipole. MLWA also overestimates the extinction efficiency for larger particles. It is possible to modify and apply

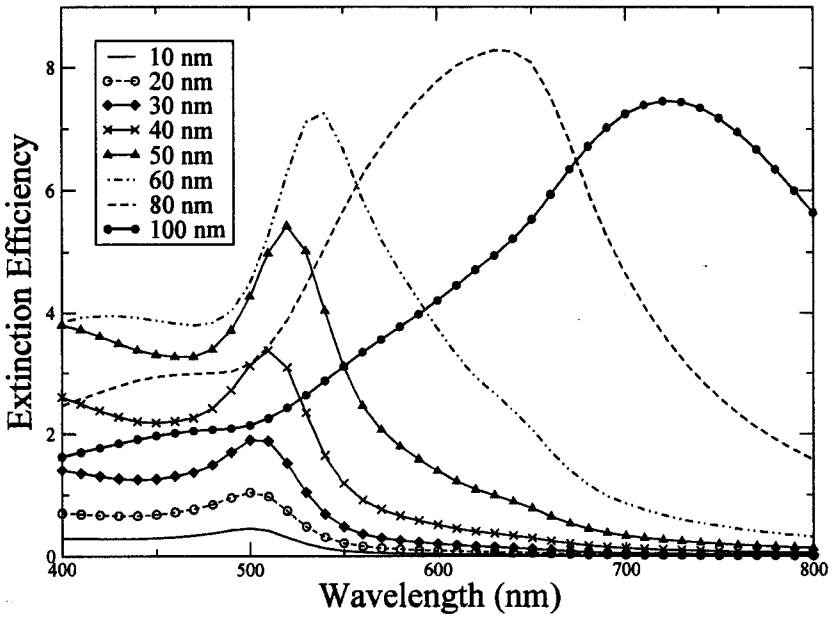

Figure 2.1: The extinction spectra for gold nanospheres with radii ranging from 10 nm to 100 nm. The calculations are done using the MLWA approximation.

MLWA for certain non-spherical particles [51, 48] by solving the electrostatic problem of scattering from a certain target, while including the radiative corrections and surface scattering effects in the dielectric constants. Zeman and Schatz [48] solved this problem for a metal prolate spheroid and included corrections to the order of λ^3. They showed for a prolate spheroid, the plasmon resonance red shifts as the ratio between the two major dimensions increases, i.e., as the spheroid becomes more needle-like. The main reason that MLWA is not appropriate for our calculations is that it is not accurate for non-spherical particles.

2.2.2 Effective Medium Theories

Another set of approximation methods are those which treat the substrate and thin film of metal nanoparticles as a whole. An example of this is the Maxwell-Garnett theory of surfaces [20] in which the optical constants of a thin film on a substrate is given in terms of an effective thickness of island and bulk metal's constants. Other examples are the R, R', T method [28] and Marton-Schlesinger's method [29] which calculate optical properties of the film and also its effective thickness using reflection and transmission coefficients. The main disadvantage of these methods is that they do not address the effect of the nanoparticle's shape, size, coating, or the interactions between nanoparticles on the LSPR.

Based on Bedeaux and Vlieger's model [30] of a surface with the so-called excess field, Lazzari and Simonsen introduced a software program [31] to calculate the linear optical coefficients for surfaces and thin layers. In this model, excess fields are the difference between the real fields (containing metal particle's on the surface) and the extrapolated field for a sharp surface i.e. a surface with no nanoparticles on it. They showed that for a thin surface ($d \ll \lambda$), the Fresnel coefficients can be given in terms of excess fields [30]. The Fresnel coefficients can also be given in terms of the number

of islands per unit of surface and single island polarizabilities that can be calculated by solving Maxwell's equation in the quasi-static regime [30]. The main disadvantages of this approach are that it does not allow us to change the direction of the incident light (i.e., only transmission spectroscopy can be modelled).

2.2.3 Time-Domain Methods

Generally speaking, there are two class of numerical approaches for solving Maxwell's equations: time-domain approaches (such as finite-difference time-domain (FDTD)) and frequency-domain methods (like DDA, T-matrix). Time-domain methods [52, 53] solve Maxwell's equation as a function of time (usually find the propagation of an input signal through time). In FDTD, for example, at each time step the value of $\mathbf{E}$ and $\mathbf{H}$ are updated at each spatial point and a new value is calculated based on the stored value of $\mathbf{E}$ and $\mathbf{H}$ at that point and its neighboring sites.

The possibility of finding the spectrum with one run makes a time-domain method a well-suited approach for many different computations. For example, FDTD is especially useful when we want to find the response of a target to a coherent broad band (e.g. gaussian) input signal. It can also be used to find resonant modes by looking for peaks in the Fourier transform of the response spectrum to the input pulse. The main advantage of this approach is that only a single calculation is needed to find the spectral response for all frequencies and evolution of the field around the target. However, there are several disadvantages to this approach. Firstly, the frequency resolution is inversely related to the simulation time and increasing the resolution needs a long run time. Secondly, for stability reasons the time step should be proportional to the spatial size step and therefore increasing the spatial resolution results in an increase in the run time. This limits the applicability of the FDTD method to nanos-

tructured surfaces, where the high surface to volume ratio requires extremely small spatial grid point separations [54].

2.2.4 Frequency Domain Methods

In my calculations, because of the need to calculate small shifts in resonance wavelength (i.e. high resolution in frequency), I chose to take advantage of a frequency domain method for plasmon resonance calculations. In this class of methods, we solve Maxwell's equations by using $\mathbf{E}_0 e^{i\omega t}$ as the input radiation. The spectra of different frequencies are added incoherently to find the scattering properties for each frequency separately. This approach is fruitful if one wants to calculate spectral properties like absorption, scattering and extinction cross sections or to find the field enhancements around targets at specific frequencies. One of the well-known frequency-domain methods used for studying scattering from metal nanoparticles is the T-matrix method [52]. In the T-matrix method, both the incident field and scattered electric fields are expanded in terms of vector spherical harmonics and the coefficients are determined by matching boundary conditions at the target's surface. The main advantage of this method is that the T-matrix only depends on the shape, size, orientation and refractive index of the target. Once one calculates this matrix for one orientation, it is possible to rotate and calculate it for any other orientation. This saves a lot of run time if we want to do a calculation on randomly oriented nanoparticles such as in a solvent [55]. The disadvantage of this method is its poor numerical stability for particles that have large a refractive index or coating (which doubles the boundary conditions) on them [55]. The approach that I used in this work is the Discrete Dipole Approximation which will be explained in the following section.

2.3 Discrete Dipole Approximation (DDA)

The Discrete Dipole Approximation (DDA), which is a well-known method, is accurate when the targets are smaller than the wavelength. It was firstly proposed by Purcell and Pennypacker in 1973 [56] to study interstellar dust grains. Subsequently, Draine and Flatau [57] developed the method and wrote a FORTRAN implementation of this technique, known as DDSCAT [57, 58], which has been now used for studying the localized surface plasmons in noble metal nanoparticles [18, 36, 46]. The DDA is the substitution of a continuum target, of arbitrary geometry, by an array of N discrete polarizable points (dipoles) at $\mathbf{r}_i$'s. Each point is assigned a polarizability α_i. When light shines on the target, the polarizable points acquire dipole moments which interact with each other. The local electric field at each point is written as a sum of the incident field and a contribution from every other dipole. This leads to a set of 3N linear equations For a finite N, it is feasible to solve the equations and calculate the scattering, absorption and extinction of the dipole array which we assume is equal to scattering properties of the continuum target. There are some issues that should be addressed when using the DDA:

1. How many dipoles do we need to approximate a continuum target with sufficient accuracy?

2. Given an array of polarizable points, how should we assign polarizabilities to each point so that we get the most accurate approximation?

3. How accurate is DDA given a target of certain size, shape and refractive index?

These issues will be addressed in the following subsections.

2.3.1 Mathematical Considerations

The dipole moment of each dipole can be given in terms of local electric field,

$$\mathbf{P}_i = \alpha_i \mathbf{E}_{loc}(\mathbf{r}_i), \tag{2.10}$$

where $\mathbf{E}_{loc}(\mathbf{r}_i)$ is the local electric field at $\mathbf{r}_i$(the location of the i^{th} dipole). Now we can write the local electric field as

$$\mathbf{E}_{loc}(r_i) = \mathbf{E}_{inc,i} - \sum_{j \neq i} \mathbf{A}_{ij} \cdot \mathbf{P}_j, \tag{2.11}$$

where

$$\mathbf{A}_{ij} \cdot \mathbf{P}_j = \frac{e^{ikr_{ij}}}{r_{ij}^3} \left\{ k^2 r_{ij} \times (r_{ij} \times P_j) + \frac{(1 - ikr_{ij})}{r_{ij}^2} \times [r_{ij}\mathbf{P}_j - 3\mathbf{r}_{ij}(\mathbf{r}_{ij} \cdot \mathbf{P}_j)] \right\} \quad (j \neq i). \tag{2.12}$$

Here $k = \omega/c$, $\mathbf{E}_{inc}(\mathbf{r}_i) = \mathbf{E}_0 e^{i\mathbf{k}\cdot\mathbf{r}_i}$, $\mathbf{r}_{ij} = (\mathbf{r}_i - \mathbf{r}_j)$.

Now if we define $\mathbf{A}_{ii} \equiv \alpha_i^{-1}$, the problem will reduce to a set of $3N$ complex linear equations:

$$\sum_{i=1}^{N} \mathbf{A}_{ji} \cdot \mathbf{P}_i = \mathbf{E}_{inc}(\mathbf{r}_j) \tag{2.13}$$

Solving the above equations for the $\mathbf{P}_j$'s we can calculate the electric field at the site of each dipole using equation 2.10. We can also find scattering, absorption and extinction efficiencies of the target. The mean power removed from the incident field by each dipole is equal to $-\frac{1}{2} Re(\mathbf{P}_i \cdot \dot{\mathbf{E}}^*_{inc}(\mathbf{r}_i))$ [50], so one can find the extinction cross section from the following equation:

$$\mathbf{C}_{ext} = \frac{4\pi k}{|\mathbf{E}_0|^2} \sum_{j=1}^{N} Im(\mathbf{P}_j \cdot \mathbf{E}_{inc}(\mathbf{r}_j^*)). \tag{2.14}$$

Also, since the instantaneous power radiated by a dipole [59] is

$$\left(\frac{dE}{dt}\right)_{sca} = \frac{\omega^4}{3c^3} \mathbf{P} \cdot \mathbf{P}^*, \tag{2.15}$$

it follows that the power absorbed is equal to

$$\left(\frac{dE}{dt}\right)_{abs} = \frac{\omega}{2}\left\{Im[\mathbf{P}\cdot\mathbf{E}^*_{loc}] - \frac{2}{3}k^3\mathbf{P}\cdot\mathbf{P}^*\right\}, \tag{2.16}$$

allowing one to calculate the absorption cross section [59]

$$\mathbf{C}_{abs} = \frac{4\pi k}{|\mathbf{E}_0|^2}\sum_{j=1}^{N}\left\{Im[\mathbf{P}_j\cdot\mathbf{E}^*_{loc}(\mathbf{r_j})] - \frac{2}{3}k^3\mathbf{P}_j\cdot\mathbf{P}^*_j\right\}. \tag{2.17}$$

For computing the scattering cross section, one can either find the electric field at far-field and integrate to find the scattered power by each dipole or simply use the equation $C_{sca} = C_{ext} - C_{abs}$. Thus the scattered electric field at the far field can be written as

$$\mathbf{E}_{sca} = \frac{k^2 e^{ikr}}{r}\sum_{i=1}^{N} e^{-ik\hat{\mathbf{r}}\cdot\mathbf{r}_j}\frac{(\mathbf{r}(\mathbf{r}\cdot\mathbf{P}_j) - \mathbf{P}_j)}{r}. \tag{2.18}$$

2.3.2 Dipole Polarizabilities

Having a lattice of points specified with a lattice spacing d, one should also assign to each dipole site a polarizability that connects the local electric field at each point to its dipole moment $\mathbf{P}_i = \alpha_i\mathbf{E}_{loc}(\mathbf{r}_i)$. In the DC limit, $(kd) \to 0$, one would use the famous Clausius-Mossotti prescription: $\alpha^{(CM)} = (3d^3/4\pi)(\epsilon-1)/(\epsilon+2)$ where $\epsilon = m^2$ is the complex dielectric constant. Draine [59] showed that for better accuracy we should take radiative corrections into account. The reason is that when an incident plane wave encounters a single real dipole, the dipole will scatter and absorb an amount of energy from the wave, and attenuate the field, which requires the dielectric constant of the medium to contain an imaginary part. To take this into account one can include another field correction and write $\mathbf{P} = \alpha^{(CM)}(\mathbf{E}_{inc} + \mathbf{E}_{rad})$ where $\mathbf{E} = (\frac{2}{3})ik^3\mathbf{P}$ [50]. Draine [59] showed this introduces a correction proportional to $O[(kd)^3]$:

$$\alpha = \frac{\alpha^{(CM)}}{1 - (2/3)ik^3\alpha^{(CM)}} = \alpha^{(CM)}\left[1 - \frac{2i}{3N}(ka^3_{eff}\frac{\epsilon-1}{\epsilon+2}\right]^2, \tag{2.19}$$

where $a_{eff} \equiv (3N/4\pi n)^3$ is the effective radius of the target. One can check that the above α approaches 0 at the limit $(kd \to 0)$ or $N \to \infty$.

Another approach is to assign a polarizability to each dipole so that an infinite lattice of dipoles has the same dispersion relation $\epsilon(\omega)$ as the bulk material. Draine and Goodman solved this problem [60] and derived the following polarizability for the long-wavelength limit:

$$\alpha^{LDR} \approx \frac{\alpha^{(CM)}}{1 + (\alpha^{(CM)}/d^3)[(b_1 + m^2 b_2 + m^2 b_3 S)(kd)^2 - (2/3)i(kd)^3]} \tag{2.20}$$

$$b_1 = -1.891531, \qquad b_2 = 0.1648469, \tag{2.21}$$

$$b_3 = -1.7700004, \qquad S = \sum_{j=1}^{3} (\hat{a}_j \hat{e}_j)^2, \tag{2.22}$$

where $\hat{a}$ and $\hat{e}$ are unit vectors defining the incident direction and the polarization state respectively.

2.3.3 Validity Criteria

There are two main validity criteria for DDA. Firstly, the number of dipoles N must be large enough to represent the continuum target completely. The second criterion is to make sure that the lattice spacing is smaller that wavelength i.e. the phase change from a dipole to its neighbor is equal or smaller than 1 radian. This criterion also makes sure that polarizabilities that we got from equation 2.22 would relate the local electric field and dipole moments correctly. The second criterion can also be formulated as $|m|kd < 1$ or equivalently

$$N > (4\pi/3)|m|^3 (ka_{eff})^3. \tag{2.23}$$

This validity criterion limits the size of the targets that can be accurately modelled by the DDA. According to our calculations, the spacing needed to achieve convergence for a gold nanoparticle at optical frequencies is 0.5 nm. This is equivalent to having means 3×10^4 dipoles for a 14 nm diameter gold nanoparticle.

2.3.4 DDSCAT

DDSCAT is a FORTRAN f77 implementation of DDA developed by B.T. Draine and J. Flatau [58] to calculate scattering, absorption, and extinction properties of an arbitrary object. All the DDA calculations reported in result chapter were done using DDSCAT6.0.

This program solves the problem of scattering and absorption from an array of polarizable points irradiated with a plane wave of monochromatic radiation. The input files needed for our target geometries were specially created. Using the input files, the appropriate incident light, and its polarization, DDSCAT computes the extinction cross section for a given wavelength by finding solving a scattering problem of a plane wave with the given wavelength and from the target, which is modelled by a lattice of dipoles. DDSCAT has been previously used for calculating and studying the absorption and scattering properties of noble-metal nanoparticles by different groups [36, 18, 46].

2.3.5 Computational Complexity and Scaling of DDSCAT

Discrete Fourier Transform (DFT) and Complex Conjugate Gradient (CCG) are two different iterative approaches that DDSCAT uses to solve the set of $3N$ linear equations 2.13 [61, 62]. For DFT, DDSCAT uses the well-known Fastest Fourier Transform in the West (FFTW) package developed by Frigo and Johnson in MIT [63]. Goodman, et al. [64] showed that for N dipoles on a periodic lattice, FFT can be used to solve the equation 2.13 in $O[3Nlog(3N)]$ operations instead of $O[(3N)^2]$ which is the number of operations that it takes if one uses CCG method. Since N can be large this is an important step and makes some infeasible problems feasible.

To use the FFT method the assigned array should be rectangular. Therefore,

for an arbitrary target, the program extends the target to a rectangular lattice and solve the problem of scattering from the extended target instead. This may lead to an increase in needed memory while running the program. The memory requirement of FFT is proportional to the number $N_{FFT} = N_x N_y N_z$ of sites in the extended "computational volume". Only for a rectangular target is this number equal to N the number of actual dipoles in the target. For targets of other geometries, $N_{FFT} > N$. For example, for a spherical target $N_{FFT} \approx (6/\pi)N$ or for a tetrahedron $N_{FFT} \approx 6N$. Using 8 bytes per complex number, DDSCAT requires approximately $1.0 + 0.61(N_{FFT}/1000)$MB thus a 32^3 computational volume needs only 21MB but a 64^3 volume would need 161 MB [65].

Most of the computing time is spent in the iterating process until the vector solution $\mathbf{P}$ satisfies equation 2.13 to the required accuracy. The time spent per iteration scales approximately as N_{FFT}. For all of our calculations we took advantage of a 1.6-GHz Itanium2 CPU available on SHARCNET: The Shared Hierarchical Academic Research Computing Network. For a 7 nm radius gold sphere with the light of wavelength $\lambda = 800nm$, the calculation took 3200 CPU-seconds for N=139000. For a dimer of two similar spheres and a 17.4 nm center-to-center separation, the calculation required 5316 CPU-seconds and 6854 CPU-seconds for two polarization directions of the incident field for an extended target of N=432000 dipoles.

2.3.6 Accuracy of DDSCAT

In this section, I present the comparison between the Mie theory which is an exact theory, and results that I calculated for the same target using DDSCAT with 2×10^5 dipoles. Calculations show that DDA calculations are within 5% of Mie theory results. For wavelengths smaller than 680 nm calculations are within 1% Mie theory calculations. However for smaller particles, for a gold sphere with a radii of 20 nm

DDA overestimates the extinction efficiency for wavelength larger than 680 nm by a factor of 2 but the promising point is that DDA keeps the overall shape and resonance locations very accurately (*within* 0.1 %) as seen in Fig.2.2. The next chapter

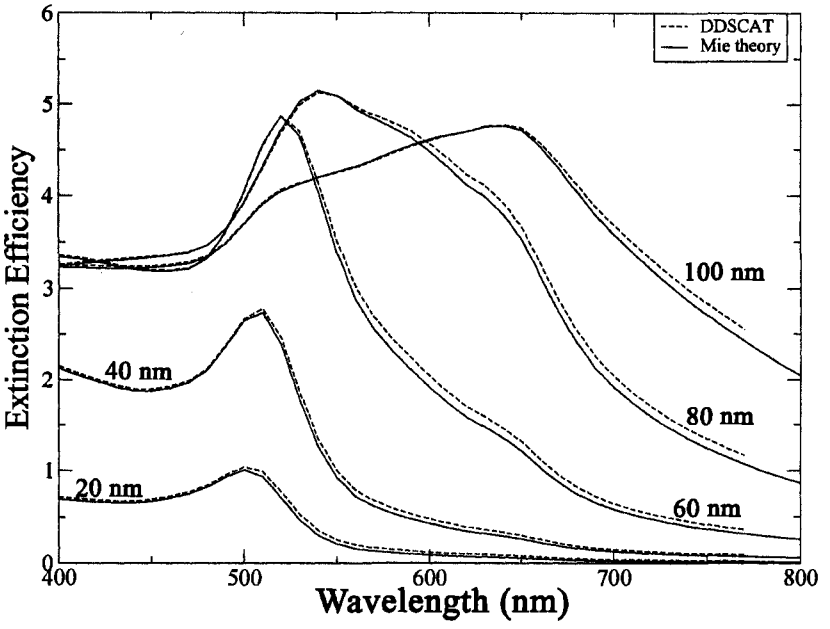

Figure 2.2: Extinction efficiency vs. wavelength for gold spheres with radii ranging from 20 to 100 nm. Comparison of the DDSCAT calculations with Mie theory calculations.

presents the results of my DDA calculations of the LSPR of arrays and aggregates of hemispherical gold nanoparticles.

Chapter 3

Results, Discussion and Conclusion

In this chapter, I present calculations for localized surface plasmon resonance spectra for different gold nanoparticle arrays and aggregates immobilized on a surface of a waveguide. In addition, I present calculations for the electric field around these nanoparticles at specific frequencies. All the calculations reported here are for gold nanoparticles with radii of 7 nm unless otherwise mentioned, and were performed using DDSCAT. The nanoparticle shapes are hemispheres that model experiments using OMCVD deposited nanoparticles [24]. The wave vector of the light is always along the supporting surface of nanoparticles, on which nanoparticles are immobilized, as shown in Fig. 3.9, and this models the geometry in Evanescent Waveguide Absorption Spectroscopy (EWAS) [66, 67] experiments. The polarization of light is linear, and is either perpendicular to the supporting surface (P polarization), or parallel (S polarization) to the supporting surface. In the following sections, I first study

the effect of a dielectric coating on the spectrum of a dimer of closely-spaced gold nanoparticles. By calculating the electric field around the dimer, I show that the physical origin of the spectral features is the electric field enhancement between the two nanoparticles. I then present the effect of a dielectric coating on the spectra of three nanoparticles arranged in both a cluster and linear chain. This result indicates that the spectrum of nanoparticles arranged in a linear array show a larger response to the addition of a dielectric coating. This hypothesis is confirmed by the calculation of the spectrum of a linear array of four nanoparticles that are coated by a dielectric. Then I present the calculation of the electric field amplitude around a dimer of gold nanoparticles. Based on these results, I propose a novel method of detecting a small concentration of biomolecules on a linear array of gold nanoparticles.

3.1 Effect of a Dielectric Coating on LSPRs in Dimers

In this section, I study the effect of putting a dielectric coating on a dimer of gold nanoparticles. The following calculations are motivated by an experiment and a calculation reported in [36]. In a search to develop a new biosensing approach, the experimenters attached biomolecules (biotin-streptavidin) on to gold nanoparticles that are placed randomly on the surface of a waveguide. The radiation has two different polarizations, one that is perpendicular to the surface of the waveguide (P polarization) and another which is parallel to the surface of the waveguide (S polarization). They found that the EWAS spectra was modified by this coating of biomolecules only in the S polarization.

As seen in the Fig. 3.1, there is a redshift in the plasmon peak as biomolecules are attached on the nanoparticles. In addition, when using S polarized light, there

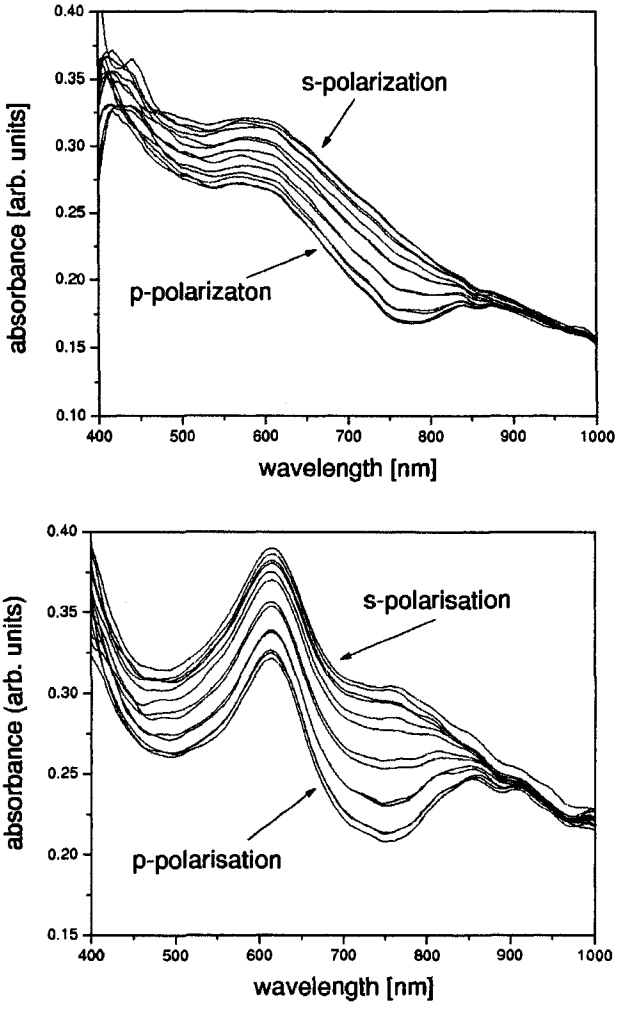

Figure 3.1: Measured EWA spectra of 40 min-grown nanoparticles of first generation with successively changed polarization in 15 steps: 0 and 180 represent a pure TE (s-polarized) mode whereas 90 represents a pure TM (p-polarized) mode. (top) without coating and (bottom) with a 1,8 octanedithiol SAM. Reprinted figure with permission from Patrick Rooney, Asad Rezaee, Songbu Xu, Touraj Manifar, Abdollah Hassanzadeh, Ganna Podoprygorina, Volker Böhmar, Chitra Rangan and Silvia Mittler, Physical Review B, **77**(23):235446, 2008, Copyright(2008) by American Physical Society.

is a second peak present in the absorption spectra of the coated particles that is missing from the spectra when using P polarized light. In order to explain the basic feature of this experiment, Rooney, et al. used a simple model of two adjacent gold nanohemispheres. When the nanoparticles have the biomolecules attached, this was modeled by a dielectric coating layer. The extinction spectra for different separations in both the coated and uncoated cases was calculated. As seen in the Fig. 3.2, for closely-spaced dimers, in addition to the redshift in the main peak in the spectrum, there is another peak that grows as the separation in the dimer decreases, provided the polarization of light is along the interparticle axis. The second peak, which is called the 'cross-talk' peak, dies away rapidly as the separation between two nanoparticles increases. Rooney, et al. also showed that the presence of a dielectric layer on the nanoparticles allowed the cross-talk peak to last for even larger separations than for an uncoated dimer. This effect called "optical clustering".

I examined the effect of a dielectric coating on the extinction spectra of a dimer of closely-spaced gold nanohemispheres. Fig. 3.3 shows the extinction efficiency spectra for a dimer of gold nanohemispheres. The first noticeable feature is a 10-20 nm redshift in the resonance peak which can be seen for both polarizations. This is a common feature seen when the effective radius of the target increases or the ambient refractive index increases. As observed by Rooney et al. [36], another feature is a second peak around 630 nm which can only be seen when using S polarized light and is enhanced if the nanoparticles are coated with a dielectric layer. In the next section, I show that this second peak is a result of the electric field enhancement between the two particles. Note that magnitude of the extinction efficiency for the S polarized light is much bigger than the P polarized light. The reason is that for P polarization the number of dipoles (scatterers) along the polarization direction is small. However, for the other polarization (S polarization), because dipoles are located along

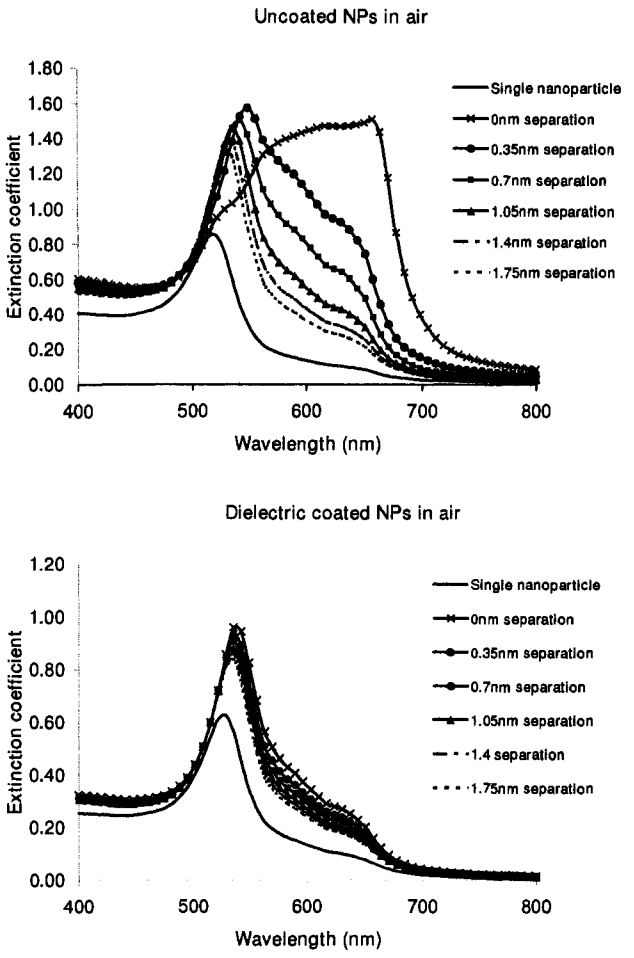

Figure 3.2: Calculated extinction spectra for two hemispherical gold nanoparticles with varying interparticle separations. Particles are (top) uncoated in air and (bottom) coated in air. All coatings have a refractive index of 1.45. The particle radius is 7 nm and coating thickness is 1.75 nm. Separation is measured as distance between surfaces, which for coated particles means the coating-to-coating distance. The radiation is in S polarization. Reprinted figure with permission from Patrick Rooney, Asad Rezaee, Songbu Xu, Touraj Manifar, Abdollah Hassanzadeh, Ganna Podoprygorina, Volker Böhmar, Chitra Rangan and Silvia Mittler, Physical Review B, **77**(23):235446, 2008, Copyright(2008) by American Physical Society.

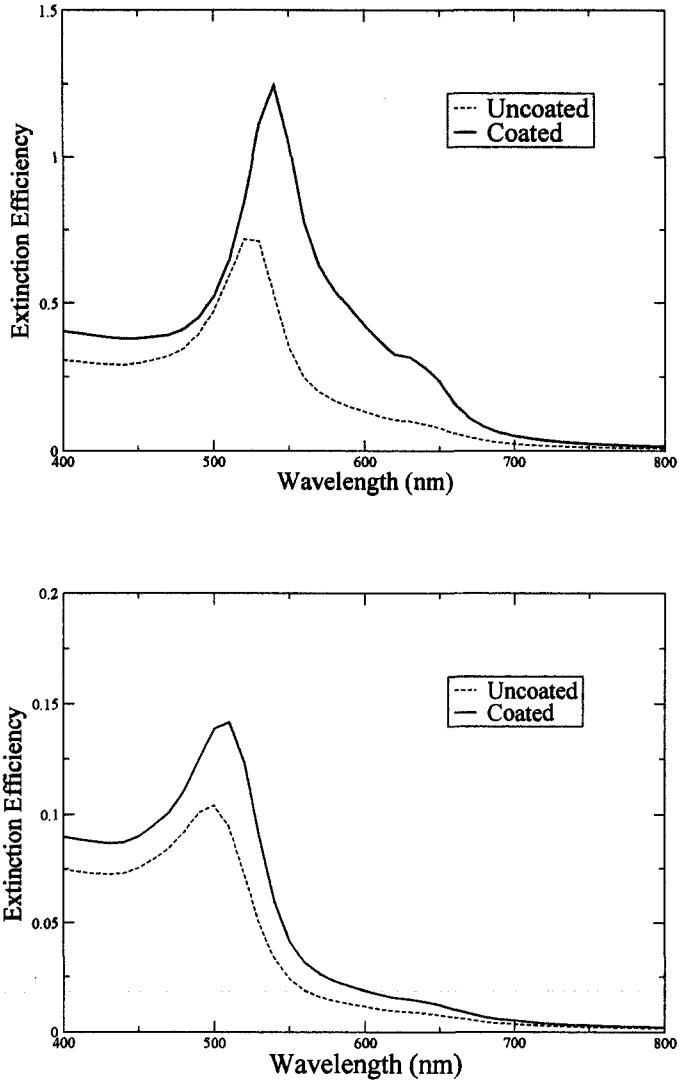

Figure 3.3: Extinction efficiency vs. wavelength for a dimer consisting of coated and uncoated gold nanohemispheres with radii of 7 nm. The center-to-center separation is fixed at 17.5 nm. The coating layer is 1.75 nm thick. The refractive index of the coating layer is 1.45. The top panel presents S polarization and the bottom panel P polarization.

the polarization direction, the electric field "sees" dipoles and the extinction cross section (and extinction efficiency) increases.

3.2 Electric Field Calculations around a Dimer

In this section, I present the calculation of the electric field around a dimer of gold nanohemispheres and provide a physical mechanism for the appearance of the cross-talk features.

Fig. 3.4 shows the relative ($|E_{coated}|/|E_{uncoated}|$) electric field at each point on the waveguide surface and outside the nanoparticles for P polarization. The wavelength of light is $\lambda = 630\ nm$ corresponding to the appearance of the cross-talk peak. Figure 3.5 shows the same calculation for S polarization (i.e. ratio of the electric field is along the inter particles axis). Fig. 3.6 presents the calculation of the relative electric field (i.e. the electric field after coating to the electric field before coating) at each point between two gold nanohemispheres (along $y = 17.5$ nm) with light at a wavelength of $\lambda = 630nm$. It shows that, if the light polarization is along the inter-particle axis, the electric field gets enhanced by a factor of 2$\sim$3.

This confirms the hypothesis [36] that the origin of optical clustering is indeed the enhancement of the electric field in between the particles mediated by the dielectric coating. But when the polarization of light is perpendicular to the chain, the electric field is suppressed. It is therefore possible to switch between field enhancement and suppression at the same point (between two coated gold nanohemispheres, by changing the light polarization).

This can be explained in a simple classical picture. When the nanoparticles are irradiated by light, to leading order, their charge oscillations set up an induced dipole

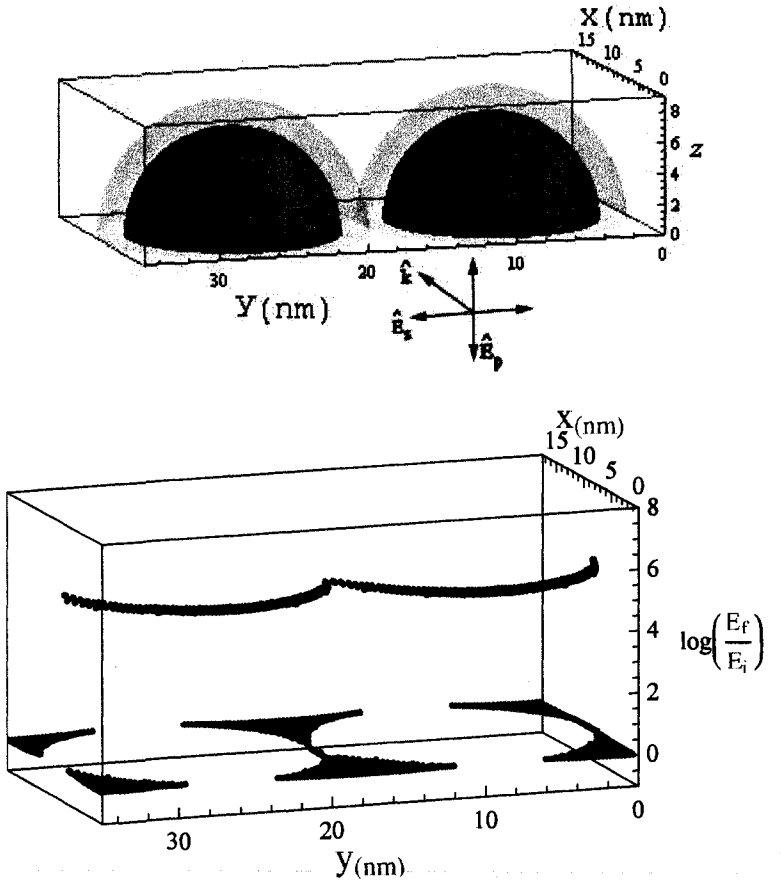

Figure 3.4: Schematic diagram of the target and incident field orientation (top). Change in the electric field intensity due to the dielectric coating ($\log[\frac{E_f}{E_i}]$) outside the two nanoparticles and on the plane of support (z=0) of the two nanohemispheres P polarization (bottom) of the incident light.

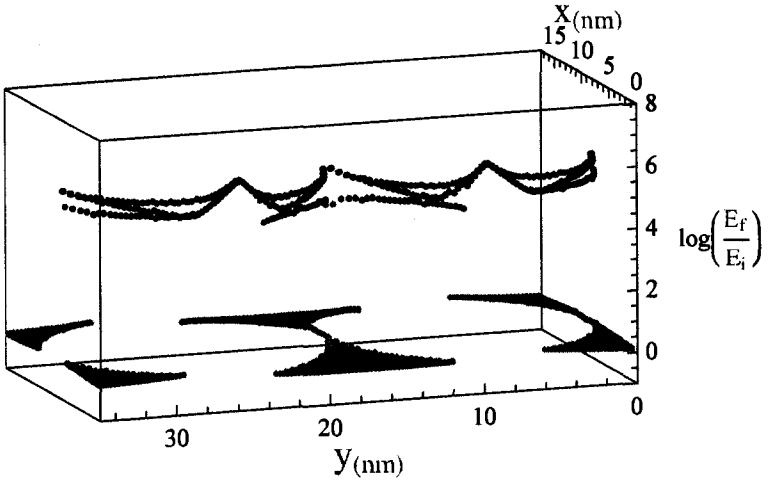

Figure 3.5: Change in the electric field intensity due to the dielectric coating ($\log[\frac{E_f}{E_i}]$) outside the two nanoparticles and on the plane of support (z=0) of the two nanohemispheres for S polarization (bottom) of the incident light.

parallel to the electric field polarization. Adding the coating on the nanoparticles leads to a longer (due to the increased size), but weaker (because of the dielectric coating layer on the nanoparticle) dipole. For S polarized light, these two dipoles are aligned and therefore the electric field between two dipoles is enhanced. For P polarized light, however, the weaker dipoles are parallel to each other. Therefore the electric field between the two nanoparticles is reduced.

As seen in figures ??, There is a region for both polarizations of light in which the magnitude of the electric field increased drastically. These points are called hot spots. At the hot spot regions, closer to the incident field, the presence of the coating has enhanced the electric field by a factor of 10^5. Thsi results shows how to prepare a surface especially for surface enhanced processes (e.g. SERS [44]) in a much more effective manner rather than relying on the random hot spots formed when using self-assembled or deposited nanostructures on surfaces.

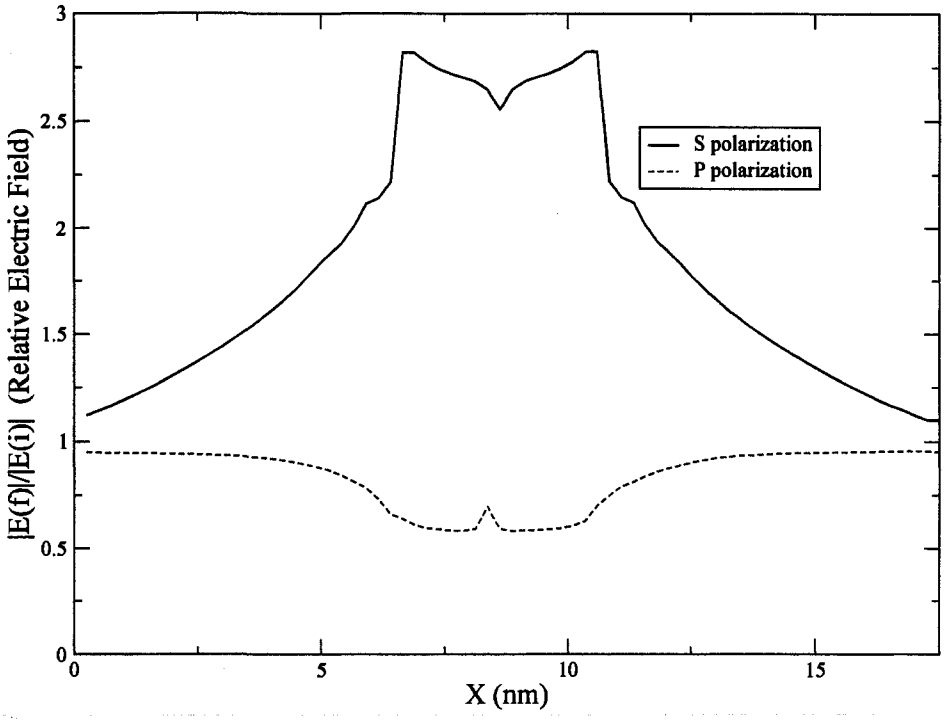

Figure 3.6: $\frac{|E_f|}{|E_i|}$ at each point on the intersection of the plane of support of two hemispheres and the surface bisecting two hemispheres (at $y = 17.5$).

3.3 Effect of Aggregation and Arraying

Adding a third particle to a dimer can lead to either a linear chain or a cluster and these two arrangements exhibit different LSPR spectra. In this section, I present the calculations for these two kinds of geometry, and compare the effect of coating on their LSPR. In dimers, a second peak (cross-talk) shows up (only in S polarization), as the nanoparticles approach together. Cross-talk dies away quickly (exponentially), when the particles are separated [35], but the presence of a coating can bridge separations, and the cross-talk peak lasts for longer separations [36].

Figure 3.7 shows the extinction spectra for a cluster of three hemispheres. The center-to-center separation is either 19.25 nm or 17.5 nm and the light polarization is along the surface on which hemispheres are placed. Cross-talk also shows up when a dielectric coating is put on the nanoparticles (S polarization). The ratio of the cross-talk peak to the first peak (dipolar peak), is less than 0.25 for a separation of 19.25 nm and is about 0.3 for a separation of 17.5 nm. Note that a limitation of using DDA for this calculation is that we ignore the additional electric field component along the $\hat{k}$ vector in the TM mode of the waveguide, so the results are approximate.

The other way to add the third nanoparticle, is to add it at the end of dimer and make a linear chain of three nanoparticles. Figure 3.8 shows the extinction spectra for a chain of three coated and uncoated nanohemispheres. Here the ratio of the cross-talk peak to the dipolar peak is 0.41 which is bigger than the same quantity for the previous cluster. This can be explained by noting that here there are two plasmon couplings between neighboring particles along the electric field directions. However, for a nonlinear cluster, the dipole field of the nanoparticle in the back row does not overlap with the dipole moment of particles in the front row, and this avoids the full coupling between nanoparticles.

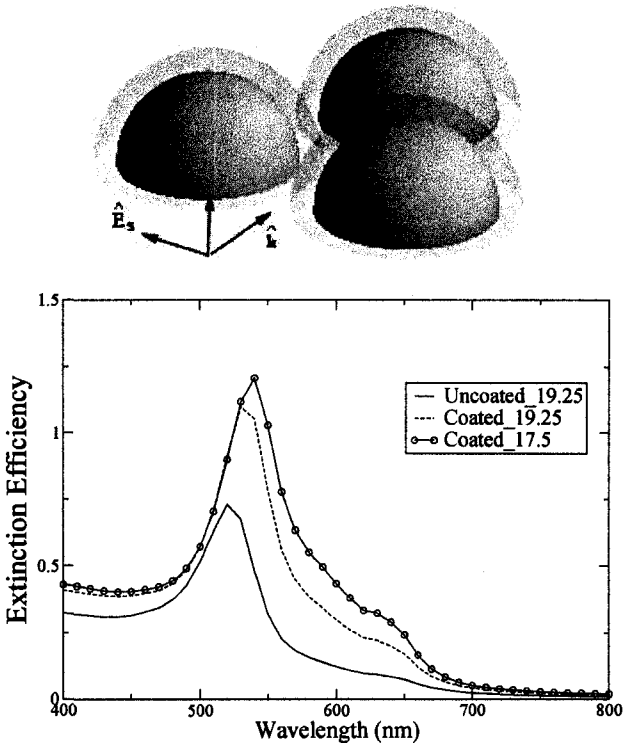

Figure 3.7: (top) The geometry of target and radiation's orientation. (bottom) Extinction efficiency vs. wavelength for a cluster of three coated and uncoated gold nanospheres with radii of 7 nm. The coating has a thickness of 1.75 nm and refractive index of n=1.45. The center-to-center separation is 17.5 nm.

Another key point is the role of coating. It induces cross-talk features in the spectrum at even larger separations than the uncoated case, because the presence of a coating on the particles enhances the electric field between two neighboring nanoparticles, an effect called "optical clustering" [36]. This is an effect that can be used to implement a new biosensing approach.

3.4 A Novel Biosensing Approach Based on Immobilized Gold Nanoparticles

Based on the results of the previous section, I propose a new approach for detecting the presence of biomolecules on a linear array of nanoparticles. In this approach, gold nanoparticles are immobilized on a surface of a waveguide and an evanescent field excites the plasmon oscillations in the nanoparticles. Immobilizing nanoparticles on a surface of a waveguide provides several advantages. Because it is a 2-dimensional approach, it is possible to develop a so-called lab-on-a-chip so that the amount of a sample needed for sensing is less than the amount of a sample one would have had to use to do a usual 3D sensing, and multiple analytes can be simultaneously detected (multiplexing). Figure 3.9 shows a schematic of an experiment's setup and definitions of different light polarizations. A light source will be placed in front of the waveguide and spectrometer behind it. The evanescent field excites the plasmon oscillations in nanoparticles immobilized on its surface.

In contrast to the usual transmission-absorption spectroscopy [68, 69], because light propagates along the waveguide surface, there are two distinguishable radiation polarizations. This allows two distinct modes of interrogating the nanoparticle array, and introduces the possibility of improving the signal to noise by eliminating the systematic noise.

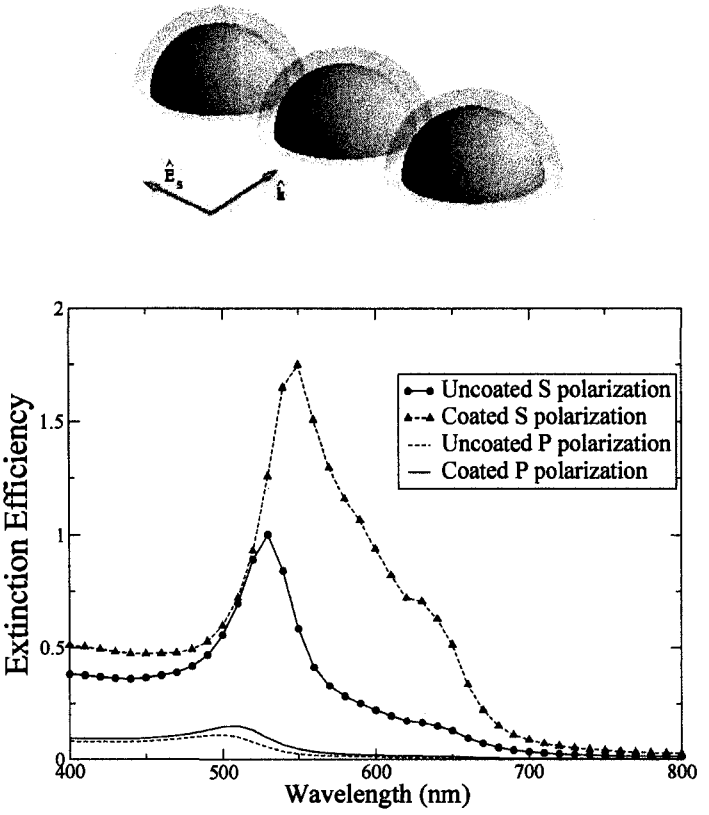

Figure 3.8: (top) The geometry of target and radiation's orientation. (bottom) Extinction efficiency vs. wavelength for a chain of 3 coated and uncoated gold nanospheres with a radius of 7 nm. The coating has a thickness of 1.75 nm and refractive index of n=1.45. The center-to-center separation is 17.5 nm.

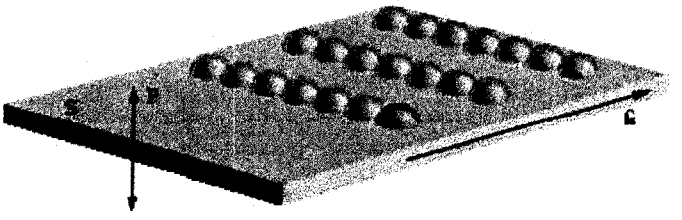

Figure 3.9: A diagram of how particles are placed on the waveguide.

Figure 3.10 shows the extinction spectrum for chains of different numbers of hemispheres. When the polarization of light is along the supporting surface, cross-talk happens in the neighboring nanoparticles in the chain, and as the number of nanoparticles increases, the ratio of the cross-talk peak to the first peak (at 500-550 nm) increases, as seen in Fig.3.11. Thus, the presence of a coating layer (model of biomolecules attached on to the gold nanoparticles), can be detected by the observation of the broadening in the spectrum from a narrow single particle spectrum to a nanowire-like one.

3.4.1 Sensitivity of the Proposed Biosensing Scheme

The sensitivity of this scheme to the change in the refractive index of the coating layer was also studied. Fig.3.12 shows that the dipolar peak moves slightly as the refractive index of the coating increases. However, the ratio of the height of two peaks changes more significantly with the refractive index of the analyte. As seen in the inset of figure 3.12, the ratio of two peak heights changes almost linearly with approximately a slope of 1.35/RIU. Fig. 3.14 shows the extinction spectrum for a linear array of spherical gold nanoparticles. It is seen that, for a chain of spheres, the proposed sensing approach is not as effective as a chain of hemispherical nanoparticles. The reason is that, in case of hemispheres, there is a broken symmetry in the system which leads to an enhancement of the electric field between two particles.

3.4.2 Effect of Nanoparticle's Shape on Biosensing Scheme

Figure 3.15 shows the spectrum for a dimer of *spheres* of the same radius ($r = 7$ nm). As can be expected from this earlier argument, for P polarization the extinction

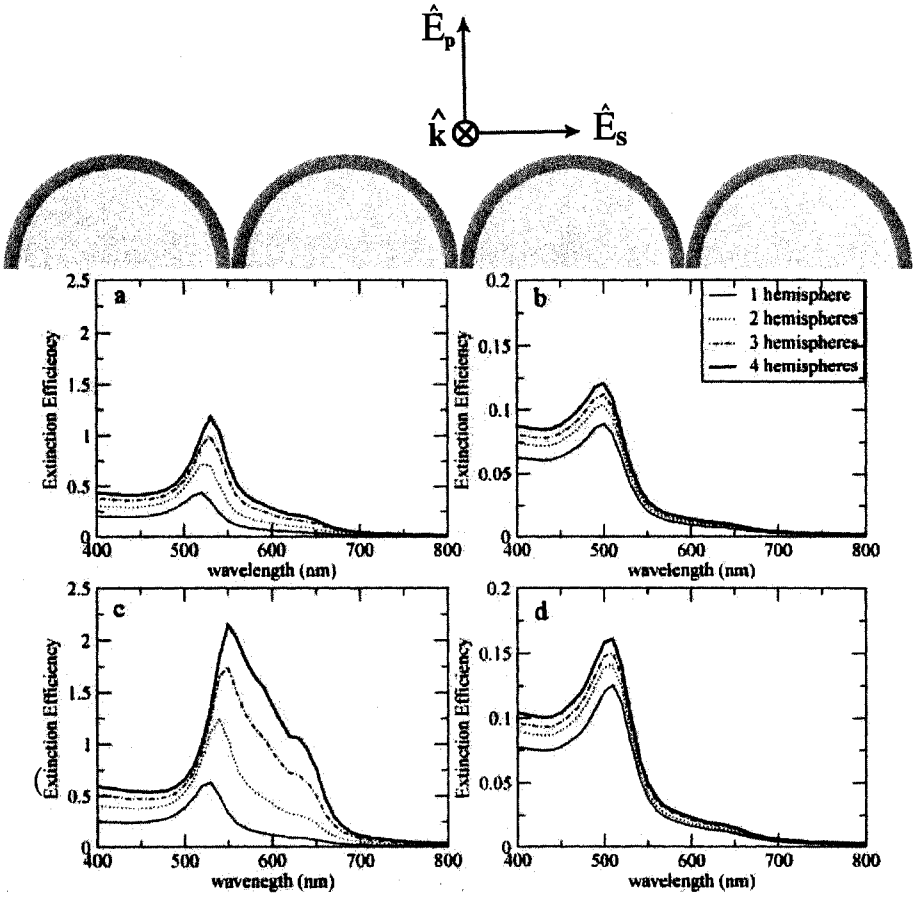

Figure 3.10: Extinction efficiency vs. wavelength for gold nanoparticle chains with different number of particles, when light polarization is along the interparticle axis (S polarization) - left two subgraphs, and when light polarization is perpendicular to the waveguide surface (P polarization) - right two subgraphs. The extinction spectra change from the uncoated spectra (a) and (b) to the spectra when coated by a dielectric analyte layer (c) and (d). The radius of all the hemispherical nanoparticles is 7nm and the thickness of coating layer is 1.75 nm. The refractive index of the coating is n = 1.45. The interparticle spacing is 17.5nm center-to-center.

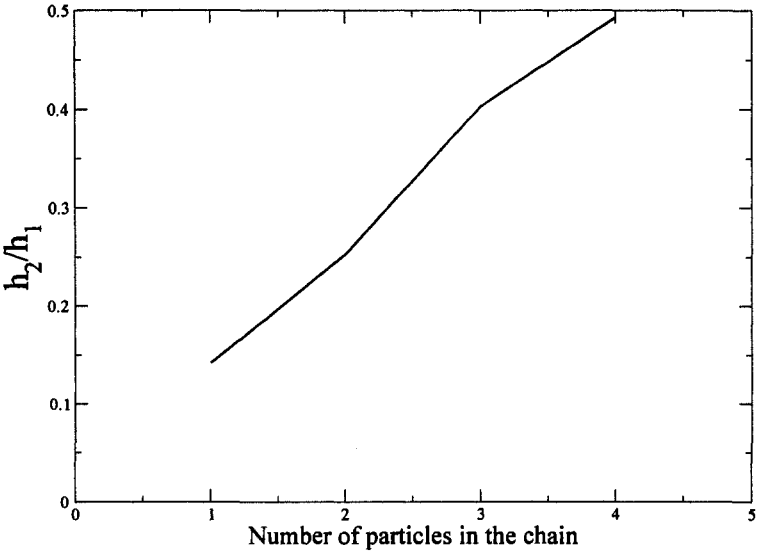

Figure 3.11: the relative height of the second peak at $\sim 630\ nm$ to the first peak $\sim (530 - 550\ nm)$ vs. the number of particles in the chain.

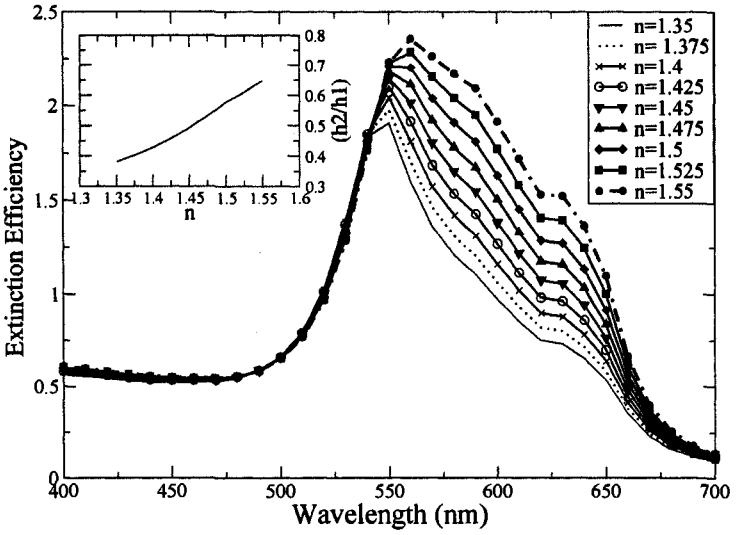

Figure 3.12: Extinction efficiency vs. wavelength for a linear chain of four hemispherical gold nanoparticles coated with different coating whose refractive indices ranging between n=1.35 and n=1.55. The particle radius is 7 nm and the thickness of the coating layer is 1.75 nm. The radiation is S polarized.

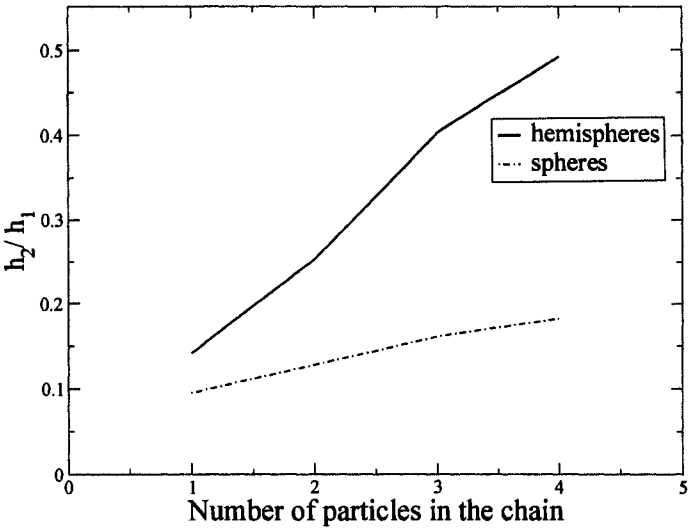

Figure 3.13: the relative height of the second peak at $\sim 630\ nm$ to the first peak $\sim (530 - 550\ nm)$ vs. the number of particles in the chain.

efficiency increases as compared to the hemispheres because of the increase in the number dipoles that the P component of the electric field "sees". The height of the second peak (cross-talk peak) is smaller than in the case of the hemispheres.

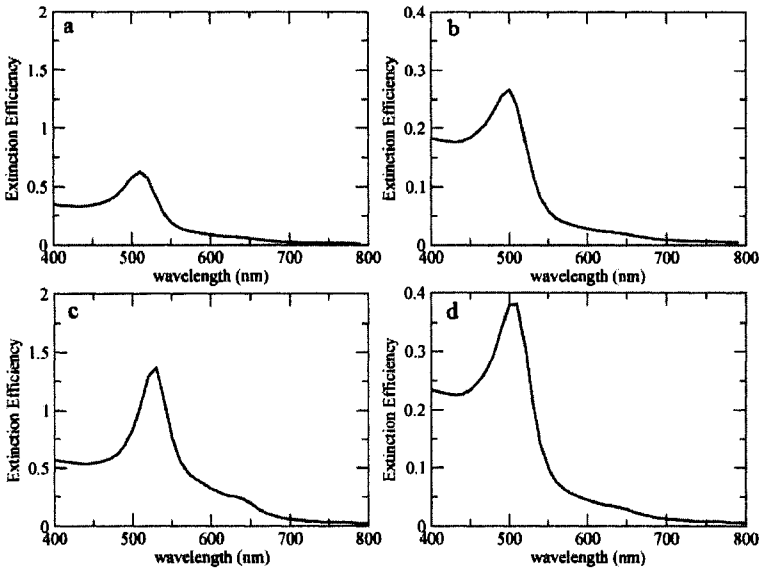

Figure 3.14: Extinction efficiency vs. wavelength for a chain of four gold nanospheres, when light polarization is along the interparticle axis (S polarization) - left two subgraphs, and when light polarization is perpendicular to the waveguide surface (P polarization) - right two subgraphs. The extinction spectra change from the uncoated spectra (a) and (b) to the spectra when coated by a dielectric analyte layer (c) and (d). The radius of all the hemispherical nanoparticles is 7nm and the thickness of coating layer is 1.75 nm. The interparticle spacing is $17.5nm$ center-to-center.

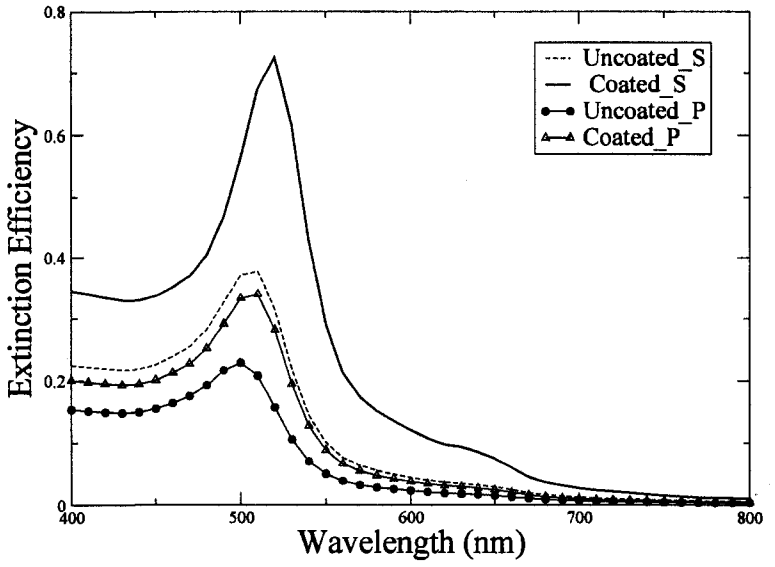

Figure 3.15: Extinction efficiency vs. wavelength for a dimer consisting of coated and uncoated gold nanospheres with radii of 7 nm. The coating layer is 1.75 nm thick. The refractive index of the coating layer is 1.45. The center-to-center separation is 17.5 nm.

3.5 Summary of Contributions

This thesis offers the following original contributions.

- Modification of the DDSCAT program in order to explore electric field magnitude at each point in the targets.
- Writing FORTRAN codes to provide the input file for targets used for the calculations.
- Reproduced all theoretical calculations of ref. [36]. In this process, I pointed out a mistake in the calculation of the extinction efficiency that led to the authors to redo all their calculations.
- Calculating the electric field between two coated gold nanohemispheres to confirm Rooney, et al.'s hypothesis [36] about the origin of the second peak in the spectrum.
- Calculating the extinction spectra for chains and clusters of closely-spaced coated and uncoated gold nanoparticles immobilized on the surface of a waveguide.
- Proposed a new biosensing approach for detecting the presence of biomolecules attached to a periodic chain of closely-spaced gold nanoparticles.
- The key results of this thesis have been included in a manuscript for publication.

3.6 Conclusion

In this work, I studied the effect of a dielectric coating on the LSPR spectra of closely spaced gold nanoparticles. For a linear array of hemispherical gold nanoparticles a coating leads to a redshift in the plasmon resonance. If the radiation polarization is along the direction of chain, it also leads to a new spectral feature at a wavelength of ~ 630 nm. It is shown the onset of this cross-talk peak is the result of an increase in the electric field enhancement between the two nanoparticles.

Based on our calculations, I propose a new approach for sensing the presence of a dielectric coating (model of recognized biomolecules) on the chain. This scheme works better for hemispherical nanoparticles than for spherical nanoparticles.

A future direction of study will be to study the effect of a substrate on field enhancements around nanoparticles. Another potentially important feature to investigate is the effect of different 2D arraying on LSPR and field enhancements. A third important avenue would be the extension of effective medium methods such as the Bedeaux-Vlieger method [30] to nanoparticle coatings and the EWAS geometry.

References

[1] M. Faraday. The Bakerian Lecture: Experimental Relations of Gold (and Other Metals) to Light. *Philosophical Transactions Series I*, 147:145–181, 1857.

[2] I.H. El-Sayed, X. Huang, and M.A. El-Sayed. Surface plasmon resonance scattering and absorption of anti-EGFR antibody conjugated gold nanoparticles in cancer diagnostics: Applications in oral cancer. *Nano Letters*, 5(5):829–834, 2005.

[3] X. Huang, I.H. El-Sayed, W. Qian, and M.A. El-Sayed. Cancer cell imaging and photothermal therapy in the near-infrared region by using gold nanorods. *Journal of the American Chemical Society*, 128(6):2115–2120, 2006.

[4] A.K.R. Lytton-Jean, M.S. Han, and C.A. Mirkin. Microarray detection of duplex and triplex DNA binders with DNA-modified gold nanoparticles. *Analytical Chemistry*, 79(15):6037–6041, 2007.

[5] A.J. Haes, S. Zou, G.C. Schatz, and R.P. VanDuyne. Nanoscale optical biosensor: Short range distance dependence of the localized surface plasmon resonance of noble metal nanoparticles. *Journal of Physical Chemistry B*, 108(22):6961–6968, 2004.

[6] C. N. R. Rao, U. Kulkarni Giridhar, P. J. Thomas, and P. P. Edwards. Metal nanoparticles and their assemblies. *Chemical Society Reviews*, 29:27–35, 2000.

[7] A. Ulman. *An introduction to ultrathin films.* Academic Press: San Diego, London, 1991.

[8] L. H. Dubois and R. G. Nuzzo. Synthesis, structure, and properties of model organic surfaces. *Annual Review of Physical Chemistry*, 43(1):437–463, 1992.

[9] A. Otto. Excitation of nonradiative surface plasma waves in silver by the method of frustrated total reflection. *Zeitschrift fur Physik*, 216:398–410, August 1968.

[10] C. F. Bohren and D. R. Huffman. *Absorption and scattering of light by small particles.* Wiley Interscience, 1983.

[11] L. Novotny and B. Hecht. *Principles of Nano-Optics.* Cambridge University Press, 2006.

[12] R. J. Green, R. A. Frazier, K. M. Shakesheff, M. C. Davies, C. J. Roberts, and S. J. B. Tendler. Surface plasmon resonance analysis of dynamic biological interactions with biomaterials. *Biomaterials*, 21:1823–1835, 2000.

[13] U. Kreibig and M. Vollmer. *Optical Propeties of metal clusters.* Springer, 1995.

[14] S. Link and M. El-Sayed. Size and temperature of the plasmon absorption of colloidal gold nanoparticles. *Reviews of Modern Physics*, 103:4212–4217, 1999.

[15] G. Mie. Beiträge zur Optik trüber Medien, speziell kolloidaler Metallösungen. *Annalen der Physik*, 330:377–445, 1908.

[16] U. Kreibig and C. V. Fragstein. The limitation of electron mean free path in small silver particles. *Zeitschrift fur Physik*, 224:307–323, August 1969.

[17] A. Kawabata and R. Kubo. Electronic Properties of Fine Metallic Particles. II. Plasma Resonance Absorption. *Journal of the Physical Society of Japan*, 21:1765–1772, September 1966.

[18] T. Jensen, L. Kelly, A. Lazarides, and G. C. Schatz. Electrodynamics of noble metal nanoparticles and nanoparticle arrays. *Journal of Cluster Science*, 10:295–317, 1999.

[19] T. R. Jensen, M. L. Duval, K. L. Kelly, A. A. Lazarides, G. C. Schatz, and R. P. Van Duyne. Nanosphere lithography: Effect of the external dielectric medium on the surface plasmon resonance spectrum of a periodic array of silver nanoparticles. *Journal of Physical Chemistry B*, 103(45):9846–9853, 1999.

[20] J. C. Maxwell Garnett. Colours in metal glasses and in metallic films. *Philosophical Transactions of the Royal Society of London. Series A, Containing Papers of a Mathematical or Physical Character*, 203:385–420, 1904.

[21] L.M. Liz-Marzan, M. Giersig, and P. Mulvaney. Synthesis of nanosized gold-silica core-shell particles. *Langmuir*, 12(18):4329–4335, 1996.

[22] S. Xu, G. Podoprygorina, V. Böhmer, Z. Ding, P. Rooney, C. Rangan, and S. Mittler. Tetraurea calix[4]arenes with sulfur functions: synthesis, dimerization to capsules, and self-assembly on gold. *Organic and Biomolecular Chemistry*, 5:558–568, 2007.

[23] C. Winter, U. Weckenmann, R. A. Fischer, J. Käshammer, V. Scheumann, and S. Mittler. Selective nucleation and area-selective OMCVD of gold on patterned self-assembled organic monolayers studied by afm and xps: A comparison of omcvd and pvd. *Chemical Vapor Deposition*, 6:199–205, 2000.

[24] A. K. A. Aliganga, A.-S. Duwez, and S. Mittler. Binary mixtures of self-assembled monolayers of 1,8-octanedithiol and 1-octanethiol for a controlled growth of gold nanoparticles. *Organic Electronics*, 7:337–350, 2006.

[25] C. Vieu. Electron beam lithography: resolution limits and applications. *Applied Surface Science*, 164:111–117, 2000.

[26] J. P. Marton and M. Schlesinger. The nucleation, growth, and structure of thin Ni-P films. *Journal of the Electrochemical Society*, 115(1):16–21, 1968.

[27] A.V. Kabashin, M. Meunier, C. Kingston, and J.H.T. Luong. Fabrication and characterization of gold nanoparticles by femtosecond laser ablation in an aqueous solution of cyclodextrins. *Journal of Physical Chemistry B*, 107(19):4527–4531, 2003.

[28] P.-O. Nilsson. Determination of optical constants from intensity measurements at normal incidence. *Appl. Opt.*, 7(3):435–442, 1968.

[29] J. P. Marton and M. Schlesinger. Optical constants of thin discontinuous nickel films. *Journal of Applied Physics*, 40(11):4529–4533, 1969.

[30] D. Bedeaux and J. Vlieger. *Optical Properties of surfaces.* Imperial College Press, 2001.

[31] R. Lazzari and I. Simonsen. Granfilm: a software for calculating thin-layer dielectric properties and fresnel coefficients. *Thin Solid Films*, 419(13):124–136, 2002.

[32] Ingive Simonsen, Rémi Lazzari, Jacques Jupille, and Stéphane Roux. Numerical modeling of the optical response of supported metallic particles. *Phys. Rev. B*, 61(11):7722–7733, 2000.

[33] M. Duval Malinsky, K.L. Kelly, G.C. Schatz, and R.P. Van Duyne. Nanosphere lithography: Effect of substrate on the localized surface plasmon resonance spectrum of silver nanoparticles. *Journal of Physical Chemistry B*, 105(12):2343–2350, 2001.

[34] D. L. Feldheim and C. A. Foss Jr. *Metal Nanoparticles, Synthesis, Characterization, and Applications.* Dekker, 2002.

[35] K.-H. Su, Q.-H. Wei, X. Zhang, J.J. Mock, D.R. Smith, and S. Schultz. Interparticle coupling effects on plasmon resonances of nanogold particles. *Nano Letters*, 3(8):1087–1090, 2003.

[36] Patrick Rooney, Asad Rezaee, Songbo Xu, Touraj Manifar, Abdollah Hassanzadeh, Ganna Podoprygorina, Volker Böhmer, Chitra Rangan, and Silvia Mittler. Control of surface plasmon resonances in dielectrically coated proximate gold nanoparticles immobilized on a substrate. *Physical Review B (Condensed Matter and Materials Physics)*, 77(23):235446, 2008.

[37] L. Zhao, K.L. Kelly, and G.C. Schatz. The extinction spectra of silver nanoparticle arrays: Influence of array structure on plasmon resonance wavelength and width. *Journal of Physical Chemistry B*, 107(30):7343–7350, 2003.

[38] A. A. Lazarides and G. C. Schatz. DNA-linked metal nanosphere materials: Structural basis for the optical properties. *Journal of Physical Chemistry B*, 104(3):460–467, 2000.

[39] Shengli Zou, Nicolas Janel, and George C. Schatz. Silver nanoparticle array structures that produce remarkably narrow plasmon lineshapes. *The Journal of Chemical Physics*, 120(23):10871–10875, 2004.

[40] M. Grant Albrecht and J. Alan Creighton. Anomalously intense Raman spectra of pyridine at a silver electrode. *Journal of the American Chemical Society*, 99(15):5215–5217, 1977.

[41] R. F. Aroca, R. A. Alvarez-Puebla, N. Pieczonka, S. Sanchez-Cortez, and J. V. Garcia-Ramos. Surface-enhanced Raman scattering on colloidal nanostructures. *Advances in Colloid and Interface Science*, 116:45–61, 2005.

[42] C. J. L. Constantino, T. Lemma, P. A. Antunes, and R. Aroca. Single-molecule detection using surface-enhanced resonance Raman scattering and Langmuir-Blodgett monolayers. *Analytical Chemistry*, 73(15):3674–3678, 2001.

[43] K. L. Kelly, E. Coronado, L. L. Zhao, and G. C. Schatz. The optical properties of metal nanoparticles: The influence of size, shape, and dielectric environment. *Journal of Physical Chemistry B*, 107(3):668–677, 2003.

[44] Shuming Nie and Steven R. Emory. Probing single molecules and single nanoparticles by surface-enhanced Raman scattering. *Science*, 275(5303):1102–1106, 1997.

[45] Hongxing Xu, Erik J. Bjerneld, Mikael Käll, and Lars Börjesson. Spectroscopy of single hemoglobin molecules by surface enhanced Raman scattering. *Phys. Rev. Lett.*, 83(21):4357–4360, 1999.

[46] E. Hao and G. C. Schatz. Electromagnetic fields around silver nanoparticles and dimers. *J. Chem. Phys.*, 120:357–366, 2004.

[47] S. Zou and G. C. Schatz. Silver nanoparticle array structures that produce giant enhancements in electromagnetic fields. *Chemical Physics*, 403:62–67, 2005.

[48] E. J. Zeman and G. C. Schatz. An accurate electromagnetic theory study of surface enhancement factors for Ag, Au, Cu, Li, Na, Al, Ga, In, Zn, and Cd. *J. Phys. Chem.*, 91:634–643, 1987.

[49] A. Wokaun, J. P. Gordon, and P. F. Liao. Radiation damping in surface-enhanced raman scattering. *Phys. Rev. Lett.*, 48(14):957–960, 1982.

[50] J. D. Jackson. *Classical Electrodynamics.* Wiley, 1975.

[51] D. S. Wang and M. Kerker. Enhanced Raman scattering by molecules adsorbed at the surface of colloidal spheroids. *Phys. Rev. B*, 24(4):1777–1790, 1981.

[52] P. W. Barber, R. K. Chang, and H. Massoudi. Electrodynamic calculations of the surface-enhanced electric intensities on large ag spheroids. *Phys. Rev. B*, 27(12):7251–7261, Jun 1983.

[53] P. W. Barber and S. C. Hill. *Light Scattering by Particles: Computational Methods.* World Scientific, 1990.

[54] A. Taflove and S. C. Hagness. *Computational Electrodynamics: The Finite-Difference Time-Domain Method.* 2nd ed., Artech House, Boston, 2000.

[55] M. I. Mishchenko, L. D. Travis, and D. W. Mackowski. T-matrix computations of light scattering by nonspherical particles: a review. *Journal of Quantitative Spectroscopy and Radiative Transfer*, 55:535–575, 1996.

[56] E. M. Purcell and C. R. Pennypacker. Scattering and absorption of light by nonspherical dielectric grains. *The Astrophysical Journal*, 186:705–714, 1973.

[57] B. T. Draine and P. J. Flatau. Discrete-dipole approximation for scattering calculations. *Journal of the Optical Society of America A*, 11:1491–1499, 1994.

[58] B. T. Draine and P. J. Flatau. Program DDSCAT.6.0: http://www.astro.princeton.edu/~draine/ddscat.html.

[59] B. T. Draine. The discrete-dipole approximation and its application to interstellar graphite grains. *the Astrophysical Journal*, 333:848–872, 1988.

[60] B. T. Draine and J. J. Goodman. Beyond Clausius-Mossotti - wave propagation on a polarizable point lattice and the discrete dipole approximation. *The Astrophyssical Journal*, 405:685–697, 1993.

[61] A. F. Peterson, S. L. Ray, C. H. Chan, and R. Mittra. *Numerical implementation of the conjugate gradient method and the CG-FFT for electromagnetic scattering, in Application of Conjugate Gradient Method to Electromagnetics and Signal Processing.* Elsevier, New York, 1991.

[62] P. Barber and C. Yeh. Scattering of electromagnetic waves by arbitrarily shaped dielectric bodies. *Applied Optics*, 14:2864–2872, 1975.

[63] Matteo Frigo and Steven G. Johnson. The design and implementation of FFTW3. *Proceedings of the IEEE*, 93(2):216–231, 2005.

[64] J. J. Goodman, B. T. Draine, and P. J. Flatau. Application of Fast-Fourier-Transform techniques to the discrete-dipole approximation. *Opt. Lett.*, 16:1198–1200, 1991.

[65] M. I. Mishchenko, J. W. Hovenier, and L. D. Travis. *Light Scattering by Nonspherical Particles: Theory, Measurements, and Applications.* Academic Press, San Diego, 2000.

[66] M. J. Adams. *An introduction to optical waveguides.* John Wiley: New York, 1981.

[67] R. G. Hunsperger. *Integrated Optics: theory and technology.* 4th ed. Springer: Berlin, New York, 1981.

[68] L.J. Sherry, R. Jin, C.A. Mirkin, G.C. Schatz, and R.P. VanDuyne. Localized surface plasmon resonance spectroscopy of single silver triangular nanoprisms. *Nano Letters*, 6(9):2060–2065, 2006.

[69] Graham A. Rance, Dan H. Marsh, and Andrei N. Khlobystov. Extinction coefficient analysis of small alkanethiolate-stabilised gold nanoparticles. *Chemical Physics Letters*, 460:230–236, 2008.

Appendix A

Copyright Permission

AMERICAN PHYSICAL SOCIETY
One Physics Ellipse, College Park, MD 20740 · http://www.aps.org

July 10, 2008

Seyed Mohammad Hashemi Rafsanjani
Department of Physics, University of Windsor
Windsor, ON N9B 3P4
Canada

Ref # 6627

Thank you for your permission request dated August 15, 2008. We are pleased to grant you a non-exclusive, non-transferable permission, English rights, limited to **print and World Wide Web format only**, provided you meet the criteria outlined below. Permission is for a one-time use and does not include permission for future editions, updates, additional electronic forms, databases, translations, or any other matters. Permission must be sought for each additional use. This permission does not include the right to modify APS material.

Please print the required copyright credit line on the first page that the material appears: "Reprinted (abstract/excerpt/figure) with permission from [FULL REFERENCE CITATION] as follows: authors names, journal title, volume number, page number and year of publication. Copyright (YEAR) by the American Physical Society.

The following language must appear somewhere on the website: "Readers may view, browse, and/or download material for temporary copying purposes only, provided these uses are for noncommercial personal purposes. Except as provided by law, this material may not be further reproduced, distributed, transmitted, modified, adapted, performed, displayed, published, or sold in whole or part, without prior written permission from the American Physical Society."

Provide a hyperlink from the reprinted APS material (the hyperlink may be embedded in the copyright credit line). APS's link manager technology makes it convenient and easy to provide links to individual articles in APS journals. For information, see: http://publish.aps.org/linkfaq.html.

You must also obtain permission from at least one of the authors for each separate work, if you haven't done so already. The author's name and address can be found on the first page of the published Article.

Use of the APS material must not imply any endorsement by the American Physical Society.

Permission is granted for use of the following APS material only:

- Figs. 2, 3, 4, Phys. Rev. B 77, 235446 (2008)

Permission is limited to the single title specified or single edition of the publication as follows:

- M.Sc. Thesis by Seyed Mohammad Hashemi Rafsanjani to be published by the University of Windsor

If you have any questions, please refer to the Copyright FAQ at: http://forms.aps.org/author/copyfaq.html or contact me at assocpub@aps.org.

Sincerely,

Eileen LaManca

Eileen LaManca
Publications Marketing Coordinator

VITA AUCTORIS

Seyed Mohammad Hashemi rafsanjani was born in 1983 in Kerman, Iran. He obtained his B.Sc in physics from Sharif University of Technology in Tehran,Iran in 2006. He is currently a candidate for the Master's degree in physics at the University of Windsor and hopes to graduate in Fall 2008.